Sedimentary Geology 174 (2005) 123–148

Cryptic indicators of provenance from the geochemistry of the Okavango Delta sediments, Botswana

P. Huntsman-Mapila[a,b,*], A.B. Kampunzu[c], B. Vink[c], S. Ringrose[a]

[a]*Harry Oppenheimer Okavango Research Centre, University of Botswana, P/Bag 285, Maun, Botswana*
[b]*UBO-CNRS UMR 6538 Domaines oceaniques, Institut Universitaire Européen de la Mer, 29280, Plouzané, France*
[c]*Geology Department, University of Botswana, P/Bag 0022, Gaborone, Botswana*

Received 8 December 2003; received in revised form 10 August 2004; accepted 5 November 2004

Abstract

The siliciclastic sediments of the Okavango inland Delta of northwest Botswana have a modal composition of quartz arenites and result from a complex history, including transport by river and deposition in a nascent rift basin located in a desert environment with input of aeolian sands. The geochemical composition of sediments from the Okavango Delta was determined in order to constrain the role of weathering at the source and the composition of the source rocks. The chemical analyses and the interelement ratios show a broad compositional range usually encompassing the PAAS composition. The chemical index of alteration (CIA) values and the A–CN–K diagram define an evolution trend which can be interpreted using a mixing model involving a strongly weathered component which corresponds to the sedimentary fraction transported by the Okavango River and a relatively immature component which corresponds to the aeolian sand component of the Okavango sediments. Field geological data supported by geochemical ratios involving elements with affinity for mafic–ultramafic and felsic rocks such as Th/Cr, Th/Sc, La/Sc, La/Co and Eu/Eu* support a source area including mafic–ultramafic and felsic rocks, with or without intermediate rocks. The relationships between certain elements (Cr–Ni, Na_2O–Al_2O_3, K_2O–Al_2O_3) refine the interpretation by pointing to the existence of at least three source rock end-members, including a felsic rock source and pyroxene-rich and olivine-rich mafic–ultramafic source rocks. Proterozoic granitoid–gabbro and related volcanic and ortho-metamorphic rock complexes exposed in NW Botswana and adjacent Angola and Namibia are the source rocks of the sediment component which was mixed with aeolian sand and interacted with a variable proportion of diagenetic carbonates to produce the Okavango sediments.

Keywords: Geochemistry; Provenance; Okavango Delta; Botswana

1. Introduction

The geochemical composition of siliciclastic sedimentary rocks is a sensitive indicator of provenance

* Corresponding author. Harry Oppenheimer Okavango Research Centre, University of Botswana, P/Bag 285, Maun, Botswana. Fax: +267 661835.
E-mail address: pmapila@orc.ub.bw (P. Huntsman-Mapila).

0037-0738/$ - see front matter © 2004 Elsevier B.V. All rights reserved.
doi:10.1016/j.sedgeo.2004.11.001

and weathering at the source of sediments (Taylor and McLennan, 1985; Roser and Korsch, 1988; Hassan et al., 1999; Cullers, 2000). Concentrations of major, trace and rare earth elements (REE) of sediments are well suited to constrain provenance and source rock composition. The REE are transferred with minimal fractionation from the source material into sediments (Taylor and McLennan, 1985). The negative Eu anomaly commonly recorded in felsic igneous rocks is usually detected in clastic sedimentary rocks originating from a source made of felsic rocks (Gao and Wedepohl, 1995). Elemental ratios, e.g., La/Sc, La/Co, are usually good discriminators between mafic and felsic source rocks because La, Th and Zr are more concentrated in felsic igneous rocks whereas Co, Sc and Cr have higher concentrations in mafic rocks (e.g., Wronkiewicz and Condie, 1987).

The Okavango siliciclastic sediments, which are the focus of this study, are particularly important because they occur in a large alluvial fan with a wetland which is the largest Ramsar site on earth. The sediments result from a complex history including erosion from a relatively wet hinterland in Angola, transport by river and deposition in a basin located in a semiarid environment and direct input of aeolian sands from reworked dunes in the Kalahari desert. In this paper, the term aeolian sand refers to both direct input of fresh aeolian sand and reworked aeolian sand transported into the basin by the Okavango River.

The objectives of this paper are (1) to present new chemical analyses of Quaternary siliciclastic sediments from the Okavango inland Delta; (2) to constrain the role of weathering at the source of the Okavango sediments and the composition of the source rocks for the Okavango Delta sediments excluding the aeolian sand input.

2. Geological setting

The Okavango Delta overlies Precambrian igneous–metamorphic rocks that include the following main units (Fig. 1): (1) Paleoproterozoic ~2.05 Ga augen gneiss, granites and amphibolites exposed in the Qangwa area (Kampunzu and Mapeo, unpublished data) and 2.03 Ga granulites exposed in the Gweta area (Mapeo and Armstrong, 2001); (2) Mesoproterozoic 1.2–1.0 Ga gabbros, granites, metarhyolites and metabasalts (Kampunzu et al., 1998a, 1999); (3) Neoproterozoic siliciclastic and carbonate sedimentary rocks forming a blanket above older Proterozoic rocks (Kampunzu et al., 2000; Mapeo et al., 2000); (4) Karoo Supergroup (not shown in Fig. 1), including mainly siliciclastic sedimentary rocks deposited during the Permo-Carboniferous and mafic lavas and dolerites emplaced between ca. 181–179 Ma (Carney et al., 1994; Le Gall et al., 2002).

The Okavango Basin is a Quaternary half-graben (McCarthy et al., 1993; Modisi, 2000; Modisi et al., 2000) which represents the southwestern extension of the East African rift system (Kampunzu et al., 1998b). It is located within the Kalahari Basin, which is a shallow intracontinental basin. Aeromagnetic and seismic refraction studies suggest that the maximum thickness of sediment, in excess of 300 m, occurs in northern Namibia and in the Okavango graben in Botswana (Reeves, 1978; Modisi et al., 2000). Mineralogical studies of Kalahari sands suggest that it represents an accumulation of in situ weathering products of pre-Kalahari lithologies, in addition to material transported into the basin. (Thomas and Shaw, 1991). The major part of the catchment area comprises loosely consolidated, chiefly aeolian sand of the presently active Kalahari Basin. The Okavango Delta sediments studied in this paper represent the youngest (Quaternary) stratigraphic unit of the Kalahari sedimentary basin. Potential source rocks of the Okavango Delta sediments are mainly Proterozoic granitoids, gabbros and related volcanic and orthometamorphic rocks exposed in the catchment area in Angola, northern Namibia and northern Botswana.

3. Local setting

The Okavango River enters the Makgadikgadi–Okavango–Zambezi (MOZ) rift depression (Ringrose et al., 2005) through a narrow NW–SE-trending swamp called the Panhandle (Fig. 2) before extending into a large (>12,000 km^2) inland alluvial fan (McCarthy et al., 2000). The Okavango Delta represents the terminus of a fluvial system which drains from the central highlands of Angola where annual inflow is estimated at 1.01×10^{10} m^3 measured at the apex of the Panhandle (McCarthy et al., 2000). The present fan can be divided into distinct geo-

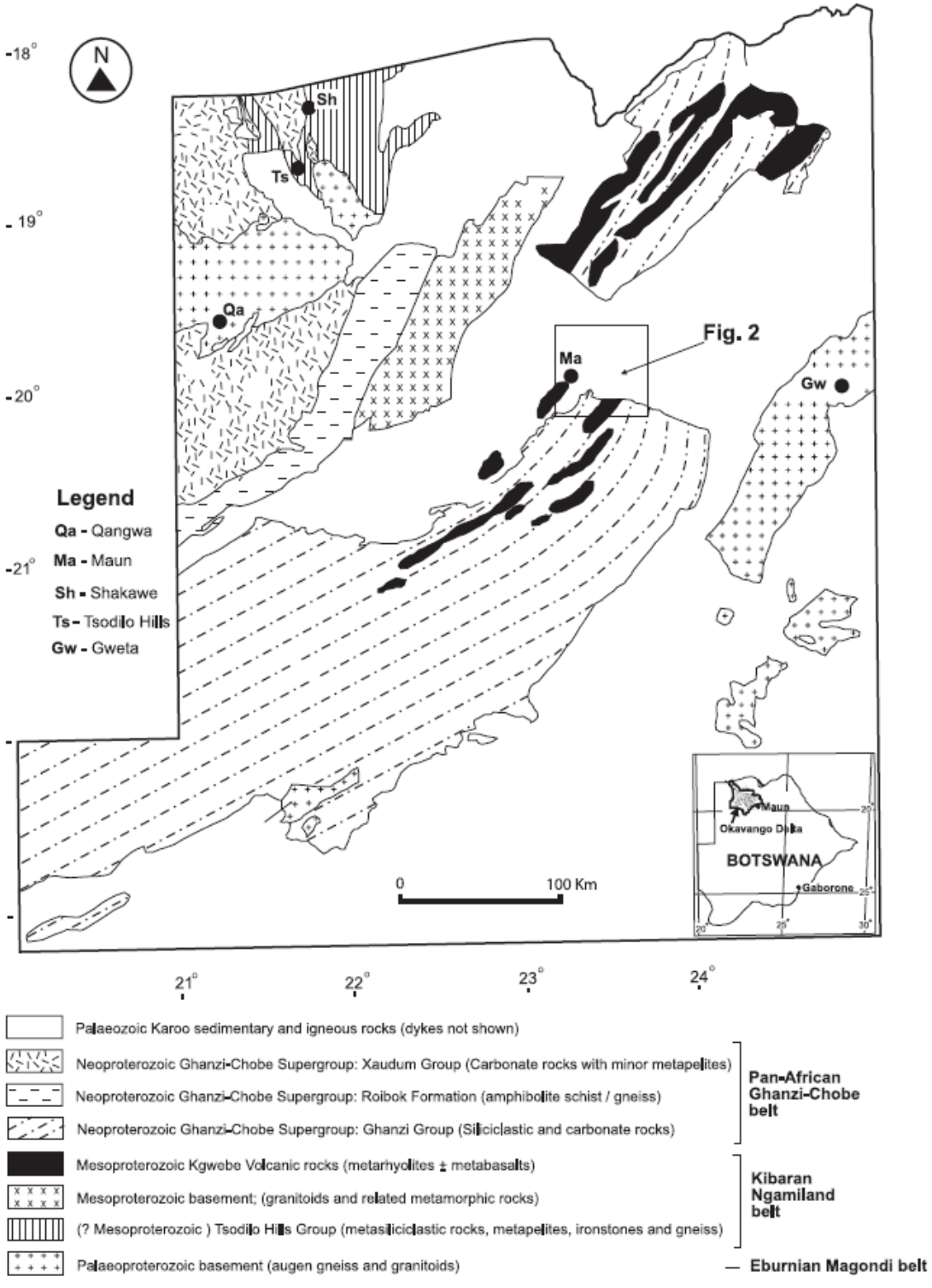

Fig. 1. Precambrian geology map of NW Botswana (Kampunzu et al., 2000). Box: location of Fig. 2 in northwestern Botswana. Insert: location of the Okavango Delta in Botswana.

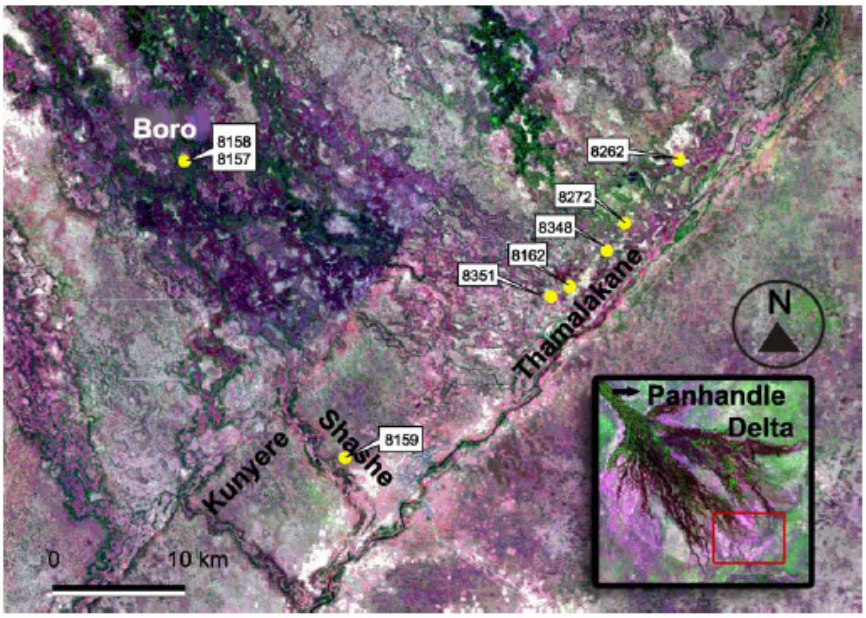

Fig. 2. Satellite image of the Okavango region showing the location of sampled boreholes. Fault zones related to the Okavango rift are prominent on this image. Insert: Okavango Delta alluvial fan morphology (courtesy of SAFARI 2000). Red rectangle: position of the main image.

morphic regions: (1) the Panhandle where the Okavango River is confined; (2) the permanent swamps; (3) the seasonal floodplains and (4) occasional (or intermittent) floodplains of the distal reaches of the Delta.

Sedimentological and geochemical evidence suggests that the wetlands of the MOZ basin have expanded and contracted over the past 400,000 years and may have been subject to extensive flooding approximately 120,000 years ago (Ringrose et al., 2005). The latest phase of contraction appears to have commenced ca. 7000 years BP (the Holocence Altithermal) and is continuing to the present day. The distal reaches of the Okavango Delta are presently a site of significant subsurface chemical precipitation of calcite and silica (McCarthy and Metcalfe, 1990). The Okavango Delta sediments contain a high proportion of sand of aeolian origin, and the floodwater constitutes the major source of the fine sediments. Airborne dust could account for the presence of clays on islands, but because the content of clay rich fines in floodplain sediments is greater than on islands, floodwater is believed to be the major source (McCarthy and Ellery, 1995). Few clastic sediments are currently introduced onto the distal reaches of the fan because of the very low gradient, dense vegetation and low suspended load of the Okavango River (McCarthy et al., 1991). Throughout the Okavango system, the current chemical sedimentation volumetrically exceeds the amount of clastic sediment being brought into the fan (McCarthy and Metcalfe, 1990).

4. Sampling and analytical procedures

Fifty-eight samples from boreholes sunk in the study area were selected for grain size (sieving) analysis performed as part of the Maun Groundwater Development Project (DWA (Department of Water Affairs), 1997). In addition, during the course of this study, grain size was determined on 42 samples taken from shallow (3 m) holes sunk in the study area (see data in Table 1). Thirteen representative samples were selected for microscope investigations conducted on a Zeiss Axioskop 40 microscope fitted with a Zeiss AxioCam MRc digital camera. Twelve representative samples were selected for X-ray diffraction analyses

Table 1
Petrographic characterisitics of the Okavango sediments

Grain size data

Location	Depth	No. of samples	Mean (phi)	Sorting
Shashe[a]	40–65 m	32	1.66	0.56
Thamalakane[a]	12–38 m	8	1.89	0.56
Thamalakane[a]	42–70 m	9	1.94	0.66
Boro[a,b]	38–65 m	3	2.18	0.57
Boro[a,b]	45–57 m	6	2.07	0.77
Shallow depth holes[c]	0–3 m	42	2.40	0.69
Shallow depth holes[d]	2–3 m		2.20	Well sorted

Microscopic and XRD data

Sample nr.	Quartz	Calcite	Dolomite	Kaolinite	K-feldspar	Muscovite	Clay[e]
8157a	96	–	–	2	2	–	–
8157f	100	–	–	–	–	–	–
8159g	93	5	–	–	Trace	2	–
8159j	28	65	7	–	–	–	–
8159n[f]	44	10	43	–	3	–	–
8159o	30	23	45	–	2	–	–
8159t	82	5	13	–	–	–	–
8262c	100	–	–	–	–	–	–
8162e	90	–	–	3	4	–	3
8162o	98	–	–	–	–	–	2
8348d	100	–	–	–	–	–	–
8348j	95	–	–	3	2	–	–

[a] DWA (1997).
[b] Split spoon sample analysis.
[c] This study.
[d] McCarthy and Ellery (1995).
[e] Clay minerals other than kaolinite.
[f] Possibly some heulandite.

using a Philips PW 3710 X-ray Diffraction unit, operated at 45 kV and 40 mA, employing Cu–Kα radiation and a graphite monochromator. The samples were scanned from 3° to 70° for 2θ, and their diffractograms were digitally recorded.

Ninety samples were collected from seven boreholes (Fig. 2) drilled during the Maun Groundwater Development Project (DWA (Department of Water Affairs), 1997) for whole rock geochemical analyses. Two boreholes (BH8157 and BH8158) are located on the lower reaches of the Boro channel, a major tributary of the Delta that has active flow throughout most of the year. This channel abuts on the distal Kunyere and Thamalakane faults which are major normal faults bounding the Okavango half-graben to the southeast (Fig. 2). The boreholes BH8351, BH8162, BH8262 and BH8348 are located along the Thamalakane River valley, and BH8159 is located in the Shashe valley, which has been dry since the early 1990s. Representative samples were obtained at 3-m intervals up to depths of between 69–147 m.

The chemical analyses of sediments were performed at Chemex Laboratories in Canada. Major elements were determined using ICP-AES. Trace and rare earth elements were analysed using ICP-MS (detection limits generally between 0.1 and 0.5 ppm) with the exception of Li, Cr, Ni and Pb that were determined by flame AAS (detection limits 1 ppm). The analyses of standards run at the same time as the studied samples are shown in Table 2. The precisions are ≤1% and ≤10% for major and trace elements, respectively. Inorganic CO_2 was determined using a Leco-Gasometric and Leco-IR detector with detection limits of 0.2%.

Table 2
Representative samples and summary of the range of chemical compositions of the Okavango Delta sediments[a]

Sample nr.	8157A	8157F	8158A	8158F	8158H	8159A	8159E	8159G	8159I	8159J	8159M	8159N
Depth (m)	3	54	6	60	90	6	45	60	69	81	99	102
SiO_2 (wt.%)	89.97	96.11	83.17	97.79	96.43	98.18	68.72	68.07	68.17	58.39	48.45	53.82
TiO_2	0.23	0.10	0.29	0.07	0.09	0.02	0.23	0.14	0.23	0.27	0.23	0.14
Al_2O_3	4.99	1.77	5.47	0.65	1.31	0.34	3.90	1.96	3.11	4.52	4.57	2.67
FeO	1.27	0.38	1.40	0.22	0.31	0.40	1.27	0.71	1.17	1.82	1.83	1.33
MnO	0.01	0.01	0.01	0.01	0.01	0.01	0.06	0.03	0.04	0.04	0.04	0.04
MgO	0.36	0.09	0.34	0.13	0.06	0.03	1.95	4.53	3.21	2.79	5.49	6.65
CaO	0.68	0.27	1.83	0.04	0.05	0.10	11.43	9.62	10.07	13.51	15.29	14.60
Na_2O	0.16	0.06	0.13	0.02	0.09	0.03	0.15	0.24	0.37	0.71	0.99	0.48
K_2O	0.49	0.21	0.50	0.13	0.22	0.10	0.59	0.72	1.08	1.68	2.46	1.67
P_2O_5	<0.01	<0.01	<0.01	0.01	<0.01	0.01	0.01	0.01	0.03	0.08	0.10	0.05
CO_2	<0.2	<0.2	<0.2	<0.2	<0.2	<0.2	6.4	9.8	7.6	10.2	14.8	16.4
LOI	–	1.47	5.86	0.75	1.11	0.76	11.19	14.09	13.04	16.94	20.73	19.21
Total	98.30	100.50	99.16	99.83	99.70	99.23	99.64	100.20	100.65	100.95	100.40	100.80
Cr (ppm)	60	11	29	6	9	4	71	1300	4	55	39	27
Ni	4.8	4.0	13.4	2.0	3.0	2.0	3.8	440	2.0	3.6	17	27
Co	40.0	46	25	45	54	64	21	21	16	15	14	16
Sc	30	<5	5	<5	<5	5	20	750	5	70	5	<5
V	75	20	90	5	15	<5	45	30	45	60	85	55
Cu	10	5	10	5	5	5	10	5	5	15	15	15
Pb	6.5	3.0	8.5	1.5	2.5	1.0	44	236	1.0	3.0	5.5	4.5
Zn	20	5	15	5	20	25	25	5	20	25	25	25
Rb	26.4	9.4	27.4	11.4	8.4	3.0	24.8	23.4	32.0	47.8	53.6	31.0
Cs	1.3	0.4	1.5	29.0	0.3	–	0.8	0.9	0.9	1.4	1.5	0.7
Ba	261	94	270	52	107	38	316	1120	1110	653	759	927
Sr	35.6	14.2	50.4	4.5	9.7	6.0	213	559	397	357	824	871
Li	14	6	15	4	6	4	17	10	12	15	31	22
Ta	11	13	5	15	18	22	5	5	4	2	2	2
Nb	8	5	6	5	7	7	6	4	5	5	4	2
Hf	3	1	9	3	1	–	3	1	3	1	1	<1
Zr	143	97	443	166	113	29	146	104	149	78	69	44
Y	9	5	15	3	4	2	10	7	10	11	9	7
Ga	6	2	7	1	<1	1	5	1	3	5	5	2
Th	3	1	5	<1	<1	<1	4	1	3	4	4	2
U	1.0	0.5	2.0	0.5	0.5	0.5	1.5	5.5	5.0	5.0	10.0	9.0
La	13.0	6.0	18.5	3.0	5.0	2.0	12.5	7.5	10.5	13.5	12.5	8.5
Ce	21.5	12.0	34.5	6.5	10.0	3.0	25.5	16.0	21.5	26.0	24.0	16.5
Pr	2.8	1.5	4.3	0.7	1.1	0.3	2.8	1.8	2.5	3.2	3.0	2.0
Nd	9.0	5.0	14.5	2.0	3.5	1.5	9.5	6.5	9.0	11.5	10.5	7.0
Sm	1.6	1.0	2.7	0.4	0.8	0.3	1.8	1.1	1.6	2.1	2.0	1.2
Eu	0.4	0.1	0.6	<0.1	0.1	0.1	0.4	0.3	0.5	0.5	0.4	0.4
Gd	1.9	0.8	3.0	0.5	0.6	0.1	1.7	1.1	1.7	2.0	1.7	1.6
Tb	0.2	0.1	0.4	0.1	0.1	0.1	0.3	0.1	0.3	0.3	0.3	0.1
Dy	1.5	0.6	2.2	0.3	0.4	0.1	1.6	0.9	1.5	1.5	1.5	1.2
Ho	0.3	0.1	0.4	0.1	0.1	0.1	0.3	0.1	0.3	0.4	0.3	0.2
Er	0.9	0.5	1.3	0.2	0.2	0.1	1.0	0.7	0.8	1.0	0.8	0.7
Tm	0.1	<0.1	0.1	<0.1	<0.1	<0.1	0.1	0.1	0.1	0.1	<0.1	<0.1
Yb	0.8	0.5	1.4	0.3	0.4	0.1	1.0	0.7	1.0	0.8	0.6	0.8
Lu	<0.1	<0.1	<0.1	<0.1	<0.1	<0.1	<0.1	<0.1	<0.1	<0.1	<0.1	<0.1

[a] All the samples are BH series boreholes shown in Fig. 2. The four digits in the sample numbers correspond to the numbers of these BH boreholes.
[b] UCC values from Taylor and McLennan (1995) except for TiO_2, Nb, Cs, Tb and Ta values from Plank and Langmuir (1998).
[c] PAAS composition from Taylor and McLennan (1985).
[d] NASC composition from Gromet et al. (1984).

8159O 114	8159T 147	8162D 15	8162E 24	8162J 45	8162K 51	8162L 54	81620 63	8262A 3	8262B 12	8262C 21	8262D 24	8262F 42	8348A 6
44.07	89.28	89.46	87.09	80.17	93.97	88.55	90.32	83.28	76.75	93.15	98.32	92.13	97.42
0.09	0.05	0.13	0.23	0.22	0.08	0.09	0.15	0.56	0.62	0.15	0.09	0.14	0.05
1.28	0.54	2.41	4.77	3.37	0.90	1.15	2.72	9.49	11.76	2.70	0.95	2.47	0.57
0.78	0.49	1.01	2.03	1.34	0.39	0.49	1.39	1.73	2.21	1.01	0.27	0.94	0.16
0.03	0.01	0.01	0.01	0.02	0.01	0.02	0.01	0.03	0.02	0.01	0.01	0.01	0.01
7.54	1.52	0.32	0.37	1.36	0.81	1.50	0.63	0.39	0.45	0.25	0.07	0.21	0.04
19.63	3.53	0.10	0.54	4.97	1.20	3.29	0.18	0.39	0.39	0.14	0.04	0.09	0.01
0.26	0.14	0.06	0.10	0.31	0.08	0.10	0.09	0.18	0.17	0.05	0.05	0.12	0.02
0.86	0.27	0.30	0.42	1.16	0.34	0.53	0.69	0.90	0.87	0.32	0.18	0.37	0.10
0.04	<0.01	–	0.03	<0.01	–	0.01	0.01	0.01	0.01	–	–	<0.01	0.01
22.2	4.2	<0.2	0.2	3.6	1.0	3.8	0.8	0.8	0.4	<0.2	<0.2	<0.2	<0.2
23.69	4.54	–	4.34	7.27	2.49	4.80	2.69	–	–	2.94	0.88	2.57	0.71
98.36	100.40	94.55	100.15	100.35	100.30	100.60	99.03	97.15	93.50	97.78	100.90	99.14	99.10
22	10	45	28	26	12	80	18	52	74	44	28	15	6
11	9.0	<2.8	1.6	2.6	0.6	3.0	10.8	17	25	24	32	5.6	4.0
10	42	16	25	27	31	41	26	22	21	23	131	33	110
<5	<5	70	15	15	10	10	5	40	40	55	40	5	5
50	10	15	55	60	40	10	35	105	145	40	10	35	10
20	5	5	5	5	5	5	5	20	20	5	5	5	<5
1.5	2.5	7.0	3.0	2.5	2.0	7.0	5.0	12	30	12	28	4.5	3.0
15	15	15	15	10	5	10	15	95	30	5	5	10	5
18.8	6.0	8.0	26.0	38.8	10.0	15.0	29.8	53.0	55.0	21.0	7.0	19.0	4.0
0.4	0.1	0.3	1.1	1.1	0.1	0.3	0.7	2.4	2.8	0.6	0.2	0.5	–
388	174	47	204	788	151	212	219	341	364	132	77	124	37
1910	215	7.0	35.2	199	101	251	16.6	44.8	50	20.0	8.0	17.4	5.0
16	6	6	12	13	5	5	9	21	25	7	3	7	3
2	14	4	6	8	11	14	9	5	4	6	46	11	39
1	4	1	6	6	4	5	5	11	12	4	14	6	12
<1	<1	–	1	3	3	1	5	6	7	3	1	2	–
37	54	32	83	136	145	109	223	272	281	124	92	117	55
6	3	2	8	9	4	6	10	19	22	6	3	6	2
<1	1	1	5	2	1	1	2	11	15	1	1	1	<1
2	<1	1	4	3	1	1	2	8	10	2	1	1	<1
12.0	1.5	0.5	1.5	2.0	1.0	1.5	0.5	2.0	4.0	0.5	0.5	0.5	<0.5
6.5	3.5	3.5	11.0	11.5	6.5	5.5	9.0	25.0	28.5	8.0	4.0	8.5	2.5
13.0	6.0	6.0	19.5	20.0	9.0	11.0	18.5	61.0	54.5	15.0	7.5	16.0	4.0
1.4	0.8	0.8	2.6	2.6	1.3	1.3	2.0	5.9	6.7	1.8	0.9	1.9	0.5
5.0	3.0	3.0	8.5	9.0	4.0	4.5	8.0	20.5	22.5	5.5	3.0	7.0	1.5
1.0	0.7	0.5	1.5	1.9	0.7	0.7	1.8	3.9	4.7	1.2	0.5	1.4	0.3
0.2	0.1	0.1	0.4	0.4	0.1	0.1	0.4	0.9	1.0	0.1	0.1	0.3	0.1
0.9	0.5	0.7	1.6	1.7	0.6	0.9	1.7	3.9	4.1	1.0	0.5	1.2	0.1
0.1	0.1	0.1	0.2	0.3	0.1	0.1	0.2	0.6	0.6	0.1	0.1	0.1	<0.1
0.9	0.4	0.3	1.2	1.3	0.4	0.9	1.4	2.9	3.6	0.8	0.5	0.8	0.1
0.1	0.1	0.1	0.2	0.2	0.1	0.1	0.3	0.6	0.7	0.1	0.1	0.1	0.1
0.5	0.2	0.2	0.7	0.8	0.3	0.6	0.9	1.9	1.9	0.6	0.3	0.5	0.1
<0.1	<0.1	<0.1	<0.1	0.1	0.1	0.1	0.1	0.3	0.3	0.1	0.1	0.1	<0.1
0.4	0.2	0.1	0.8	0.9	0.3	0.5	0.8	1.7	2.3	0.6	0.3	0.6	0.1
0.1	<0.1	<0.1	<0.1	<0.1	<0.1	<0.1	<0.1	0.3	0.3	<0.1	<0.1	0.1	<0.1

(*continued on next page*)

Table 2 (*continued*)

Sample nr.	8348B	8348C	8348D	8348E	8348F	8348G	8348H	8348J	8351C	8351F	8351I
Depth (m)	12	24	33	39	42	45	54	69	24	51	74
SiO_2 (wt.%)	97.51	98.54	99.04	98.25	91.81	93.73	81.90	74.49	95.78	89.40	67.78
TiO_2	0.08	0.40	0.65	0.57	2.73	2.53	6.91	7.01	0.87	3.50	3.75
FeO	0.22	0.13	0.31	0.24	1.21	0.81	2.15	2.76	0.29	1.22	1.40
MnO	0.01	0.01	0.01	0.01	0.01	0.01	0.01	0.04	0.01	0.01	0.03
MgO	0.05	0.03	0.06	0.05	0.25	0.27	0.73	1.32	0.07	0.32	2.24
CaO	0.01	<0.01	0.06	0.03	0.41	0.11	0.28	2.47	0.02	0.17	10.32
Na_2O	0.04	0.05	0.07	0.05	0.11	0.11	0.38	0.58	0.06	0.09	0.29
K_2O	0.14	0.09	0.13	0.1	0.32	0.36	1.14	1.53	0.21	0.48	1.31
P_2O_5	0.02	<0.01	–	0.01	0.01	0.01	0.03	0.03	0.01	0.01	0.01
CO_2	0.2	<0.2	<0.2	<0.2	0.2	0.6	<0.2	1.0	<0.2	<0.2	8.4
LOI	0.89	0.66	–	0.72	3.26	2.21	5.84	7.81	0.90	2.87	12.51
Total	99.87	99.95	100.45	99.37	100.3	100.35	99.95	98.46	98.32	98.41	100.05
Cr (ppm)	7	5	10	6	20	22	33	35	7	19	24
Ni	3.0	2.2	1.0	3.0	1.4	1.4	12.4	15.4	6.8	13	25
Co	101	98	251	108	71	49	46	23	91	32	38
Sc	5	5	10	5	10	15	5	5	5	5	5
V	15	5	10	5	35	20	130	75	10	35	45
Cu	<5	<5	<5	<5	<5	5	35	15	5	5	200
Pb	2.5	1.5	1.0	1.5	3.0	3.5	11	9	5	12	12
Zn	5	15	5	5	15	75	70	30	25	170	15
Rb	5.8	3.2	5.0	4.0	17.4	15.6	93.4	59.6	7.8	23.6	45.2
Cs	0.1	<0.1	0.1	0.1	0.6	0.4	3.0	1.7	0.2	0.7	1.1
Ba	62	38	86	57	210	179	708	491	84	173	491
Sr	6.3	3.0	7.0	6.0	18.0	11.0	79.4	89.7	6.9	17.1	408
Li	4	3	3	4	7	7	18	101	4	11	14
Ta	37	38	81	40	24	16	11	4	35	9	11
Nb	12	11	24	12	10	6	14	8	11	6	7
Hf	1	<1	–	1	1	1	5	4	1	5	10
Zr	87	48	71	69	90	67	227	172.5	91	248	467
Y	3	2	3	3	9	4	20	17	3	8	13
Ga	<1	<1	<1	<1	1	1	18	8	1	3	3
Th	<1	<1	<1	<1	3	1	10	6	1	3	4
U	<0.5	<0.5	<0.5	<0.5	2	0.5	2.5	1.5	0.5	1.0	3.0
La	4.5	4.0	5.0	4.5	14.5	7.0	33.5	21	4.0	11.0	15.0
Ce	7.0	5.0	9.5	8.5	31.5	13.5	65.0	42.5	8.0	22.0	29.5
Pr	0.9	0.6	1.2	1	3.6	1.7	8.2	5.2	0.9	2.7	3.6
Nd	3.0	2.0	3.5	3.5	12	5.5	26.0	18	3.5	9.0	12.0
Sm	0.5	0.3	0.8	0.7	2.6	0.9	5.0	3.6	0.5	1.6	2.1
Eu	0.1	0.1	0.1	0.1	0.6	0.2	1.3	0.8	0.1	0.4	0.5
Gd	0.3	0.2	0.6	0.7	2.2	0.9	4.0	3.4	0.6	1.3	2.3
Tb	<0.1	<0.1	<0.1	<0.1	0.3	0.1	0.7	0.5	0.1	0.2	0.3
Dy	0.2	0.1	0.4	0.4	1.6	0.7	3.9	2.8	0.4	1.2	1.8
Ho	0.1	0.1	0.1	0.1	0.3	0.1	0.7	0.6	0.1	0.2	0.4
Er	0.1	0.1	0.4	0.3	1	0.3	2.2	1.7	0.4	0.6	0.9
Tm	<0.1	<0.1	<0.1	<0.1	<0.1	0.1	0.3	0.2	0.1	0.1	0.1
Yb	0.3	0.1	0.2	0.3	0.7	0.3	1.6	1.5	0.4	0.6	1.2
Lu	0.1	0.1	<0.1	<0.1	<0.1	<0.1	0.3	0.2	<0.1	<0.1	<0.1

Range n=90	Mean n=90	Standard deviation	UCC[b]	PAAS[c]	NASC[d]	Accepted value for S.D.	Laboratory obtained	Laboratory obtained	Accepted value for S.D.	Laboratory obtained	Laboratory obtained
44.07–99.04	85.34	12.23	65.92	62.8	64.8	59.99	61.51	60.15	49.90	49.83	51.05
0.02–0.62	0.18	0.11	0.76	1.0	0.78	0.71	0.67	0.71	0.29	0.28	0.29
0.34–11.76	3.01	2.12	15.19	18.9	16.9	14.41	13.78	14.27	20.69	19.28	19.95
0.13–2.96	1.00	0.69	4.1	5.8	5.1	7.38	7.2	7.57	6.21	5.9	6.04
<0.01–0.06	0.01	0.01	0.08	0.11	0.06	0.11	0.14	0.15	0.11	0.11	0.10
0.03–7.54	1.06	1.53	2.2	2.2	2.85	1.69	1.72	1.82	0.54	0.50	0.51
<0.01–19.63	2.96	4.65	6.89	1.3	3.56	3.07	3.09	3.23	8.05	7.79	7.94
0.02–0.99	0.19	0.18	3.89	1.2	1.15	1.11	1.2	1.28	7.10	7.03	7.13
0.09–2.46	0.59	0.45	3.37	3.7	3.99	2.37	2.14	2.25	1.66	1.57	1.61
<0.01–0.10	0.01	0.02	0.13				0.16	0.14	0.13	0.11	0.10
<0.2–22.2	2.6	4.4	1.8				1.6	1.4	1.8	1.8	2.0
0.66–23.69	5.55	5.09	8.37				8.43	8.59	8.37	8.63	8.57
4–1300	38	139	35	110	125	74	116	115	74	113	117
1–440	12.4	47.4	20	55	58	286	292	291	286	305	284
10–251	44	34	10	23	26	18	24	23	2.5	3.0	3.0
<5–750	21	80	11	16	15	12	10	10	12	10	10
<5–145	43	30	60	150		170	180	175	5	<5	<5
<5–200	15	27		50		175	190	185	5	5	<5
<0.5–236	9	26				670	623	638	670	611	601
<5–170	21	26		85		165	210	180	95	90	90
3.2–93.4	23.2	16.1	112	160	125	84.5	86.0	88.2	55.0	53.6	50.6
<0.1–29	1.1	3.1		15		4.7	4.7	4.5	1.5	1.6	1.4
36.5–1120	291	250	550	650	636	1210	1190	1240	340	341	285
3–1910	163.5	305.9	350	200	142	238	228	254	1190	1120	1175
3–31	10	6		75		29	28	29		29	28
1.5–80.5	13	12				0.5	1.0	1.0	0.9	1.0	0.5
1–24	7	3	13.7	19		8	8	8	13	12	10
<1–10	2	2	6	5.0		4	3	3	11	9	9
28.5–467	127	72	190	210		138.0	144.5	142.5	517	547	479
1.5–21.5	7	4	22	27		24	22	23	119.0	120.0	124.5
<1–18	4	3		20		18	17	17	35	38	38
<1–10	3	2	10.7	14.6	12.3	10	7	7	1	<1	1
<0.5–12	2.0	2.2	2.8	3.1	2.7	11.1	10.5	11.5	0.8	0.5	0.5
2–33.5	9.9	5.8	30	38	32	23	22	22	58.0	54.5	56.5
3–65	19.2	12.0	64	80	73	45.0	44.5	45.5	122.0	118.5	120.0
0.3–8.2	2.3	1.4	7.1	8.9	7.9	5.2	5.3	5.4	15.0	14.3	14.4
1.5–26	8.0	4.8	26	32	33	21.0	19.5	19.5	57.0	51.5	50.5
0.3–5	1.5	0.97	4.5	5.6	5.7	4.5	3.9	4.0	12.7	11.7	11.8
<0.1–1.3	0.35	0.25	0.9	1.1	1.2	1.0	0.9	1.0	2.0	1.9	1.9
0.1–4.1	1.5	0.9	3.8	4.7	5.2	4.2	4.0	4.0	14.0	13.8	13.4
<0.1–0.7	0.2	0.1	0.64	0.77		0.7	0.7	0.7	2.6	2.7	2.4
0.1–3.9	1.2	0.8	3.5	4.4		3.8	3.6	3.8	18.2	16.8	16.3
<0.1–0.7	0.2	0.2	1	1.0		0.8	0.7	0.7	4.3	4.0	3.9
0.1–2.2	0.7	0.4	2.3	2.9	3.4	2.4	2.3	2.2	14.2	13.8	12.9
<0.1–0.3	0.1	0.04		0.40		0.4	0.3	0.3	2.3	2.0	2.0
0.1–2.3	0.7	0.4	2.2	2.8	3.1	2.3	2.1	2.3	14.8	13.3	13.6
<0.1–0.3	0.1	0.04		0.43		0.3	0.3	0.3	2.1	1.9	1.8

5. Petrography

Table 1 provides a summary of the grain size data from both drilling and split spoon samples from boreholes investigated. These data indicate an average grain size of between 1.7 and 2.2 φ, with a sorting between 0.56 and 0.77 for the different boreholes. Furthermore, the average grain size of the 42 shallow depth samples collected during this study was 2.40 φ (range 2.13–2.70), with an average sorting of 0.69. All these data are consistent with previously published grain size data of McCarthy and Ellery (1995) who pointed out that sediments from the lower Boro region of the Okavango Delta are dominated by well sorted sand of 2.2 φ average grain size.

Microscopic and X-ray diffraction data (Fig. 3 and Table 1) indicate that the studied samples contain the following minerals: quartz (28–100 vol.%), calcite (0–65 vol.%), dolomite (0–45 vol.%), K-feldspar (0–4 vol.%), kaolinite (0–3 vol.%), traces of muscovite and other clays (0–3 vol.%). XRD analysis of the sample 8159G indicates that it contains V-muscovite, in addition to the minerals reported in other Okavango sediments. Important to stress is that (1) no detrital muscovite has been observed under the microscope in this sample; (2) submicroscopic muscovite recorded in young sediments by XRD analyses is usually muscovite–smectite mixed layers (e.g., Deer et al., 1992). The existence of traces of heulandite in the sample 8159N (XRD data) is not yet well constrained. The presence of a micritic carbonate cement around quartz grains can be seen in Fig. 3c. There are no lithic fragments in the samples documented. The samples with the lowest quartz modal content (<85 vol.%) are rich in carbonates (>15 vol.%). Recalculating the modal composition in terms of quartz (Q), feldspars (F) and lithic fragments (L) result in Q≥94, F≤6% and L=0. In the Q–F–L diagram (Fig. 4); the data indicate that these sediments have the modal composition of very mature quartz arenites of continental cratonic provenance (e.g., Dickinson and Suczec, 1979). However, it is important to keep in mind that this modal composition is mainly controlled by the aeolian

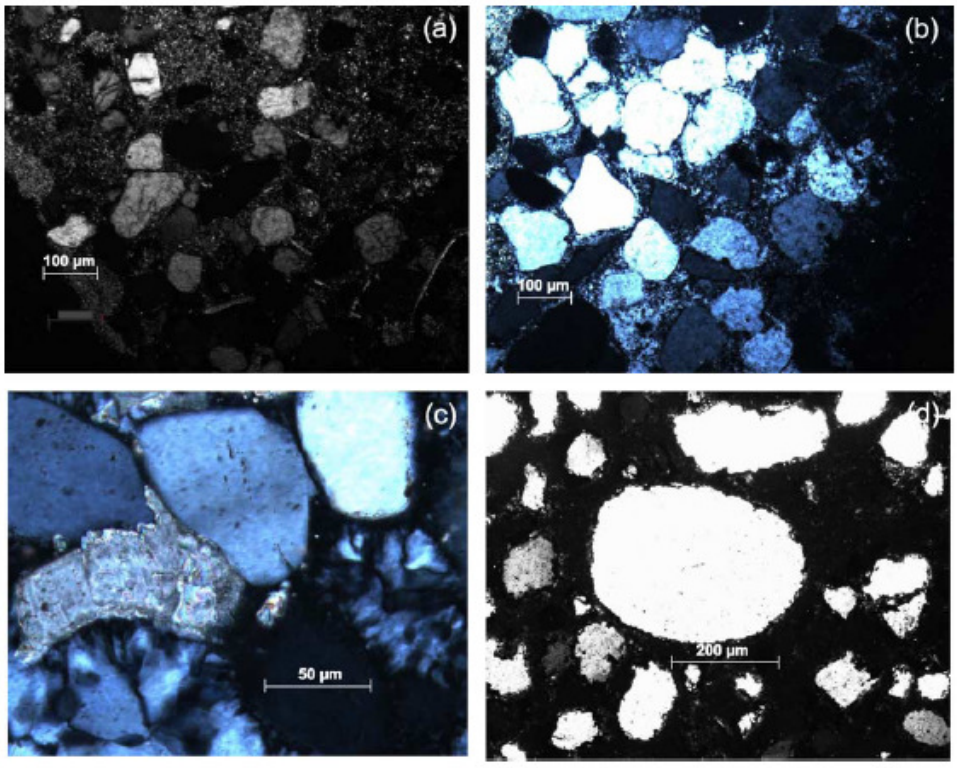

Fig. 3. Representative thin sections of Okavango sediments. (a) Sand grains (some fractured) within a carbonate cement. (b) Sand grains within a minor diagenetic silica overgrowth. (c) Micritic calcrete forming between the sand grains. (d) Sand grains showing considerable weathering on the surface.

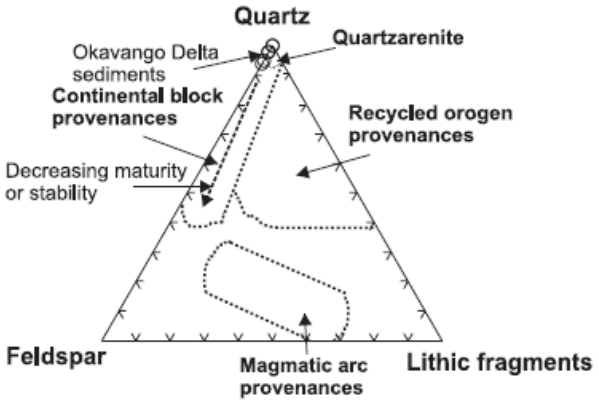

Fig. 4. Q–F–L diagram for the Okavango sediments (after Dickinson and Suczec, 1979).

sand component and is not representative of the other sediment components discussed later.

6. Major element composition

The SiO_2 content of the Okavango siliciclastic sediments ranges from 53.82 to 99.04 wt.%. Two samples, BH8159O and BH8159M, have lower SiO_2 contents (Table 2). These two samples are also marked by high concentrations of CaO, MgO and CO_2. There is a strong negative correlation between SiO_2 and Al_2O_3 when carbonate-bearing (CO_2>0.2 wt.%) samples are discarded (Fig. 5a). Al_2O_3 shows a strong

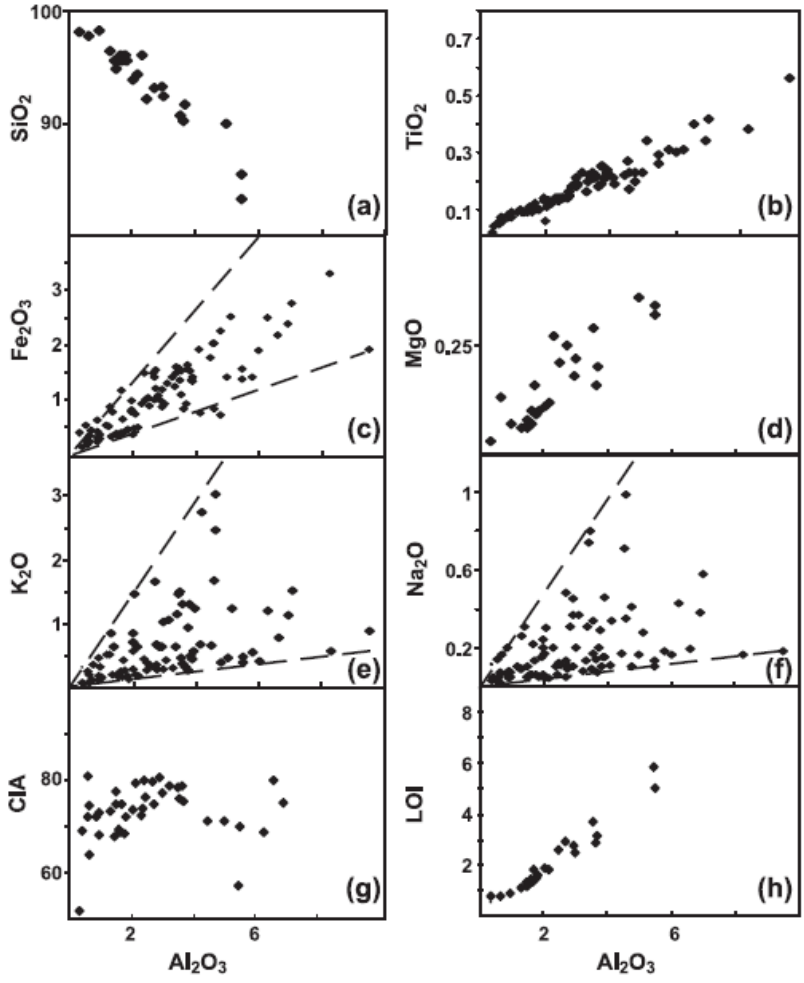

Fig. 5. Binary diagrams for Okavango sediments: major element compositions in wt.% (a) SiO_2 vs Al_2O_3; (b) TiO_2 vs Al_2O_3; (c) Fe_2O_3 vs Al_2O_3; (d) MgO vs Al_2O_3; (e) K_2O vs Al_2O_3; (f) Na_2O vs Al_2O_3; (g) CIA vs Al_2O_3; (h) LOI vs Al_2O_3.

Table 3
Representative samples and summary of the range of interelement ratios for the Okavango Delta sediments and values from other sources

Sample nr.	8157A	8157F	8158A	8158F	8158H	8159A	8159E	8159G	8159I	8159J	8159M	8159N	8159O	8159T	8162D	8162E	8162J	8162K	8162L	8162O	8262A
Depth (m)	3	54	6	60	90	6	45	60	69	81	99	102	114	147	15	24	45	51	54	63	3
Al_2O_3/SiO_2	0.06	0.02	0.07	0.01	0.01	<0.01	0.06	0.03	0.05	0.08	0.09	0.05	0.03	0.01	0.03	0.05	0.04	0.01	0.01	0.03	0.11
K_2O/Al_2O_3	0.10	0.12	0.09	0.20	0.17	0.29	0.15	0.37	0.35	0.37	0.54	0.63	0.67	0.50	0.12	0.09	0.34	0.38	0.46	0.25	0.09
CIA	71.1	68.4	57.3	74.5	73.3	51.8	–	–	–	–	–	–	–	–	79.9	–	–	–	–	–	–
Cr/Ni	13	2.8	2.2	3.0	3.0	2.0	19	3.0	2.5	15	2.2	1.0	2.1	1.1	16	14	10	12	27	1.7	3.1
Cr/V	0.8	0.6	0.3	1.2	0.6	0.8	1.6	43.3	0.3	0.9	0.5	0.5	0.4	1.0	3	0.5	0.4	0.3	8.0	0.5	0.5
Ni/Co	0.12	0.09	0.54	0.04	0.06	0.03	0.19	21.5	0.1	0.25	1.2	1.8	1.1	0.21	0.18	0.07	0.10	0.02	0.07	0.42	0.77
V/Ni	16	5.0	6.7	2.5	5.0	2.5	12	0.07	28.1	17	4.9	2.0	4.7	1.1	5.4	28	20	67	3	3.2	6.2
K/Rb	154	185	151	95	217	244	197	255	278	292	381	447	380	374	311	134	248	294	297	192	141
Rb/Sr	0.74	0.67	0.54	2.53	0.87	0.54	0.12	0.04	0.08	0.13	0.07	0.04	0.01	0.03	1.20	0.74	0.20	0.10	0.06	1.80	1.20
Ti/Zr	9.6	6.2	3.9	2.5	4.8	4.2	9.5	8.1	9.3	21	20	19	15	5.6	24.3	16.7	9.7	3.3	5.0	4.0	12.3
Cr/Zr	0.42	0.11	0.07	0.04	0.08	0.14	0.49	12.50	0.03	0.71	0.57	0.62	0.60	0.19	1.4	0.34	0.19	0.08	0.73	0.08	0.19
Y/Ni	1.9	1.1	1.1	1.3	1.2	0.8	2.6	0.02	5.9	3.1	0.52	0.26	0.57	0.33	0.71	4.0	3.3	4.0	5.8	0.9	1.1
Th/U	3.0	2.0	2.5	2.0	2.0	2.0	2.7	0.2	0.6	0.8	0.4	0.2	0.2	0.7	2	2.7	1.5	1.0	0.7	4.0	4.0
Th/Cr	0.05	0.09	0.17	0.17	0.11	0.25	0.06	<0.001	0.75	0.07	0.10	0.07	0.09	0.10	0.02	0.14	0.12	0.08	0.01	0.11	0.15
Th/Sc	0.10	0.2	1.0	0.2	0.2	0.2	0.2	<0.001	0.60	0.1	0.8	0.1	0.4	0.2	0.01	0.3	0.2	0.1	0.1	0.4	0.2
LaN/YbN	11.0	8.1	8.9	6.8	8.4	13.5	8.4	7.2	7.1	11.4	14.1	7.2	11.0	11.8	23.6	9.3	8.6	14.6	7.4	7.6	9.9
LaN/SmN	5.1	3.8	4.3	4.7	3.9	4.2	4.4	4.3	4.1	4.0	3.9	4.5	4.1	3.1	4.4	4.6	3.8	5.8	4.9	3.1	4.0
GdN/YbN	1.9	1.3	1.7	1.4	1.2	0.8	1.4	1.3	1.4	2.0	2.3	1.6	1.8	2.0	5.7	1.6	1.5	1.6	1.5	1.7	1.9
Eu/Eu*	0.70	0.34	0.64	0.60	0.44	–	0.70	0.83	0.92	0.75	0.66	0.88	0.64	0.52	0.51	0.79	0.68	0.47	0.39	0.70	0.71
Ce/Ce*	0.89	1.02	0.97	1.19	1.08	0.79	1.07	1.07	1.03	0.97	0.97	0.99	1.04	0.86	0.86	0.92	0.90	0.78	1.02	1.02	1.25
La/Sc	0.43	1.20	3.70	0.60	1.00	0.40	0.63	0.01	2.10	0.19	2.50	1.70	1.30	0.70	0.05	0.73	0.77	0.65	0.55	1.80	0.63
La/Co	0.33	0.13	0.74	0.07	0.09	0.33	0.61	0.37	0.66	0.93	0.89	0.55	0.65	0.08	0.23	0.45	0.43	0.21	0.14	0.35	1.14

[a] UCC values from Taylor and McLennan (1995) except for TiO_2, Nb, Cs, Tb and Ta values from Plank and Langmuir (1998).
[b] PAAS composition from Taylor and McLennan (1985).
[c] NASC composition from Gromet et al. (1984).

Abstract

Table 3 (*continued*)

Sample nr.	8262B	8262C	8262D	8262F	8348A	8348B	8348C	8348D	8348E	8348F	8348G	8348H	8351C	8351F	8351I	Range	Mean	Standard	UCC[a]	PAAS[b]	NASC[c]
Depth (m)	12	21	24	42	6	12	24	33	39	42	45	54	24	51	74	n=90	n=90	deviation			
Al_2O_3/SiO_2	0.15	0.03	0.01	0.03	0.01	0.01	<0.01	0.01	0.01	0.03	0.03	0.08	0.01	0.04	0.06	<0.01–0.15	0.04	0.03	0.23	0.30	0.26
K_2O/Al_2O_3	0.07	0.12	0.19	0.15	0.18	0.16	0.23	0.20	0.17	0.12	0.14	0.16	0.24	0.14	0.35	0.07–0.67	0.23	0.14	0.22	0.20	0.24
CIA	–	79.8	73.1	76.4	80.8	–	69.0	64.0	72.1	–	–	75.1	71.6	78.6	–	52–81	73	6.0			
Cr/Ni	3.0	1.8	0.9	2.7	1.7	2.3	2.3	10.0	2.0	14.2	15.7	2.7	1.0	1.4	1.0	0.88–27	5.68	6.09	1.8	2.0	2.2
Cr/V	0.5	1.1	2.8	0.4	0.6	0.5	0.4	1.0	1.2	0.6	1.1	0.3	0.7	0.5	0.5	0.3–43	1.28	4.66	0.6	0.7	
Ni/Co	1.22	1.07	0.25	0.17	0.03	0.03	0.02	<0.01	0.03	0.02	0.03	0.27	0.08	0.42	0.66	<0.01–22	0.51	2.32	2.0	2.4	2.2
V/Ni	5.8	1.7	0.3	6.3	2.8	5.0	8.0	10.0	1.7	25	14.3	10.5	1.5	2.7	1.8	0.07–67	9.37	10.13	3.00	2.7	
K/Rb	131	128	207	162	218	200	233	224	207	153	191	101	224	169	241	95–447	215	75.28	250	171	
Rb/Sr	1.10	1.00	0.86	1.10	0.73	0.92	1.10	0.69	0.71	0.97	1.40	1.20	1.10	1.40	0.11	0.01–2.53	0.92	0.5	0.32	0.80	0.88
Ti/Zr	13.2	7.3	5.9	7.2	5.5	5.5	5.0	6.0	5.3	10.7	12.6	9.0	5.3	5.1	3.2	2.5–24.3	8.82	4.43	23.9	28.5	
Cr/Zr	0.26	0.35	0.30	0.13	0.11	0.08	0.11	0.14	0.09	0.22	0.33	0.15	0.08	0.08	0.05	0.04–12.50	0.36	1.31	0.18	0.52	
Y/Ni	0.86	0.23	0.09	1.07	0.56	0.83	0.68	3.00	0.83	6.4	2.86	1.61	0.44	0.57	0.50	0.02–6.4	1.65	1.68	1.1	0.49	
Th/U	2.5	4.0	2.0	2.0	2.0	2.0	6.0	2.0	2.0	1.5	2.0	4.0	2.0	4.0	1.3	0.2–6	2.2	1.36	3.8	4.7	
Th/Cr	0.14	0.05	0.04	0.07	0.14	0.09	0.19	0.10	0.16	0.15	0.05	0.30	0.40	0.16	0.17	<0.001–0.75	0.12	0.08	0.31	0.13	0.10
Th/Sc	0.3	0.04	0.03	0.2	0.2	0.2	0.2	0.1	0.2	0.3	0.07	2.0	0.2	0.7	0.8	<0.001–2	0.3	0.32	0.97	0.91	0.82
LaN/YbN	8.4	9.0	9.0	9.6	16.9	10.1	27.0	16.9	10.1	14.0	15.8	14.1	6.8	12.4	8.4	6.8–27	10.3	3.48	9.2	9.2	7.0
LaN/SmN	3.8	4.2	5.0	3.8	5.2	5.7	8.4	3.9	4.0	3.5	4.9	4.2	5.0	4.3	4.5	3–8.4	4.22	0.75	4.2	4.3	3.5
GdN/YbN	1.4	1.4	1.4	1.6	0.8	0.8	1.6	2.4	1.9	2.6	2.4	2.0	1.2	1.8	1.6	0.8–5.7	1.74	0.64	1.4	1.4	1.4
Eu/Eu*	0.70	0.28	–	0.71	–	–	–	0.44	–	0.77	0.68	0.89	0.56	0.85	0.70	0.3–0.9	0.62	0.15	0.67	0.66	0.67
Ce/Ce*	0.99	1.02	0.99	0.96	0.91	0.85	0.75	1.02	0.98	1.11	1.00	1.01	1.00	1.02	1.01	0.75–1.3	0.98	0.08	1.1	1.1	1.1
La/Sc	0.71	0.14	0.10	0.24	0.50	0.30	0.80	0.20	0.90	1.45	0.47	6.7	0.80	3.0	3.0	0.01–6.7	1.39	1.27	2.7	2.4	2.1
La/Co	1.39	0.36	0.03	0.26	0.02	0.04	0.04	0.02	0.04	0.20	0.14	0.73	0.04	0.35	0.39	0.03–1.39	0.34	0.27	3.0	1.7	1.2

positive correlation with TiO_2 (Fig. 5b) and total Fe_2O_3 (Fig. 5c). In carbonate-free samples (CO_2<0.2 wt.%), Al_2O_3 shows a positive correlation with MgO (Fig. 5d) and LOI (Fig. 5h). There is a weak positive correlation between Al_2O_3 and K_2O (Fig. 5e) and Na_2O (Fig. 5f). In the Al_2O_3–K_2O diagram (Fig. 5e), the analyses are distributed between the lines K_2O/Al_2O_3=0.09 and 0.67. Similarly, the samples plot between the lines Na_2O/Al_2O_3=0.02 and 0.22 in the Al_2O_3–Na_2O diagram (Fig. 5f). The average K_2O/Al_2O_3 ratios of the Okavango Delta sediments is close to K_2O/Al_2O_3 ratios in the upper continental crust average composition (UCC), Post-Archaean Australian shales average composition (PAAS) and North American shale composite average value (NASC; Table 3).

The degree of chemical weathering of the source material of sedimentary siliciclastic rocks can be constrained by calculating the chemical index of alteration (CIA) of Nesbitt and Young (1982), where CIA=molar $[Al_2O_3/(Al_2O_3+CaO^*+Na_2O+K_2O)]$, CaO* being the amount of CaO in silicate minerals only (i.e., excluding carbonates and apatite). The CIA values vary from about 50 for unweathered upper crust to about 100 for highly weathered residual soils. The Okavango sediments contain variable amounts of carbonate minerals and this is reflected by variable CO_2 contents. Calcite and dolomite coexist in these rocks, and there are no microprobe data available on these minerals. Therefore, it is unrealistic to attempt correcting the carbonate-effect on the total content of CaO and MgO in the Okavango sediments. To avoid the diagenetic carbonate-effect, only samples devoid of carbonate minerals and marked by CO_2<0.2 wt.% are used in the calculation of CIA and in geochemical diagrams requiring the utilisation of CaO or MgO content in silicate minerals. The Okavango siliciclastic sediments with CO_2 <0.2 wt.% were corrected for apatite-effect using P_2O_5 values of the samples (Table 2) and yielded CIA values (Table 3) in the range 52–81 (average 73). Nesbitt and Young (1982) indicate that the influence of weathering processes at the source on the composition of clastic sediments can also be detected using the A–CN–K diagram [=molar $(Al_2O_3–(CaO^*+Na_2O)–K_2O)$] where CaO* represents the amount of CaO entering into the structure of silicate minerals. Fig. 6 shows the distribution of the carbonate-free Okavango sediments in the A–CN–K diagram. For comparison, the compositions of UCC, PAAS and NASC are also plotted in the diagram along with the predicted weathering trend for the average upper continental crust (Taylor and McLennan, 1985). This trend encompasses the majority of the Okavango samples.

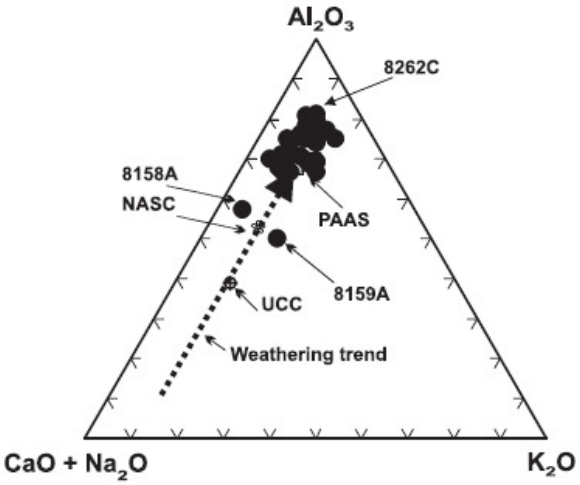

Fig. 6. A–CN–K diagram (molecular proportions) for the Okavango sediments.

7. Trace element compositions

7.1. Transition metals

The concentration of Ni in the Okavango sediments is between 1 and 32 ppm with a higher value of 440 ppm in the sample BH8159G. The Okavango sediments are marked by a large variation of cobalt, vanadium and chromium concentrations. Cr and V show positive correlations with TiO_2 and Ni (Fig. 7a–d). Ni and Cr show a positive correlation with MgO in carbonate-free samples and a weak negative correlation with SiO_2 (Fig. 7e–h). The sample BH8159G is characterised by a high concentration of Cr (1300 ppm) and high Cr/V and Ni/Co ratios (Tables 2 and 3). In contrast, it is marked by a lower V/Ni ratio. Elevated Cr and Ni abundances, as seen in sample BH8159G, were suggested by Garver et al. (1996) to reflect ultramafic rocks in the source area of sediments.

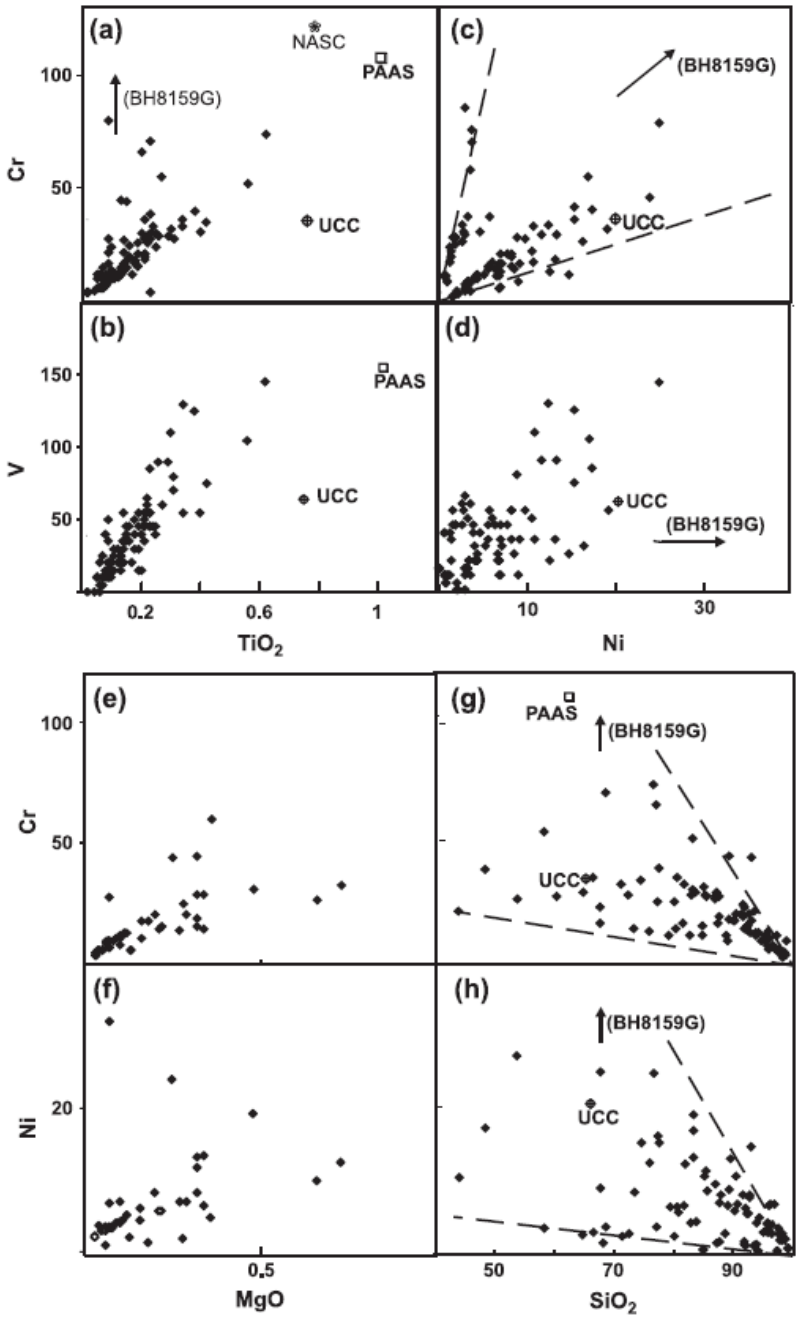

Fig. 7. Transition metal characteristics of the Okavango sediments in the plots Cr and V vs. TiO_2 (a,b); Cr and V vs. Ni (c,d); Cr and Ni vs. MgO (e,f) and Cr and Ni vs. SiO_2 (g,h).

7.2. Alkalis and alkali-earth elements

A strong positive correlation exists between K_2O and Rb (Fig. 8a). Sr shows a large range and a positive correlation with CO_2 (Fig. 8b). Rb/Sr range of carbonate-free samples encompasses the Rb/Sr ratio for PAAS. The sample BH8158F is marked by a high Cs concentration. Rb shows a strong positive correlation with Cs in carbonate-free samples (Fig. 8c). There is also a positive correlation between K_2O and

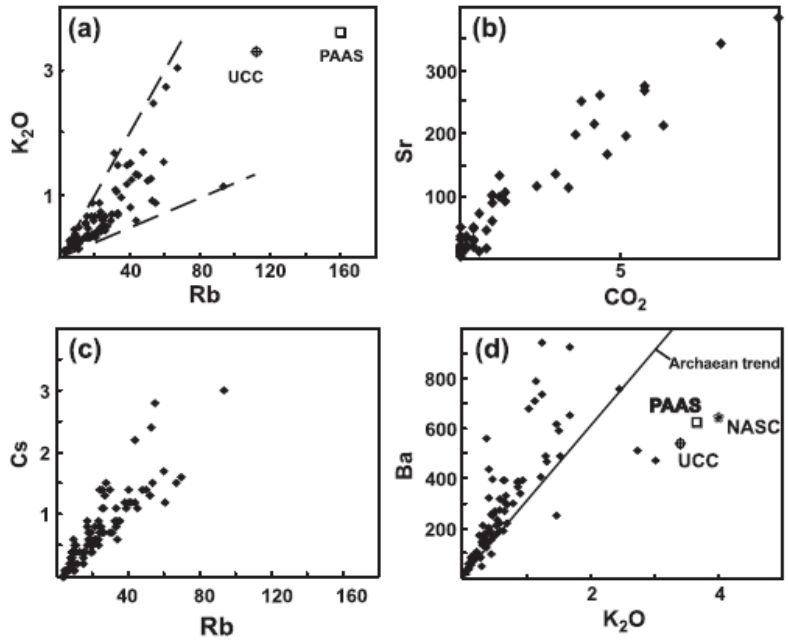

Fig. 8. Geochemical characteristics of the Okavango sediments in the binary diagrams: (a) K_2O vs. Rb; (b) Sr vs. CO_2; (c) Cs vs. Rb and (d) Ba vs. K_2O. The Archaean trend for panel (d) is from data in Lahtinen (2000).

Ba in carbonate-free samples (Fig. 8d), showing relative Ba enrichment or K_2O depletion of the Okavango sediments relative to the variation trendline in Archaean siliciclastic sedimentary rocks (e.g., Lahtinen, 2000).

7.3. High-field-strength-elements (HFSE), Th and U

Average Zr concentration in the Okavango sediments (Table 2) is 120 ppm, and fine-grained clastic sedimentary rocks are characterised by an average Zr concentration of 200±100 ppm (Taylor and McLennan, 1985). Two Okavango samples (BH8158A and BH8351I) have higher Zr concentrations between ~440 and 470 ppm (Table 2). The average Zr/Hf ratio of the Okavango sediments deduced from the Zr–Hf correlation curve is ~38 (Fig. 9). This value is similar to chondritic values and to Zr/Hf ratios in Archaean and Proterozoic sedimentary rocks in Southern Africa (Wronkiewicz and Condie, 1987; Toulkeridis et al., 1999; David et al., 2000).

Ti/Zr ratios for the Okavango sediments (Table 3) are lower than values commonly recorded in mafic igneous rocks (usually>>50), whereas felsic igneous rocks are characterised by lower values of <20. Cr/Zr and Y/Ni ratios for the Okavango samples overlap the range of values reported in both mafic and felsic igneous rocks. Cr/Zr in igneous rocks is usually >1 for mafic and <0.5 for felsic rocks. The ratio Y/Ni is lower in mafic igneous rocks (<1) than in felsic igneous rocks (>10 except in some extensional granites/rhyolites). The Nb concentrations are high

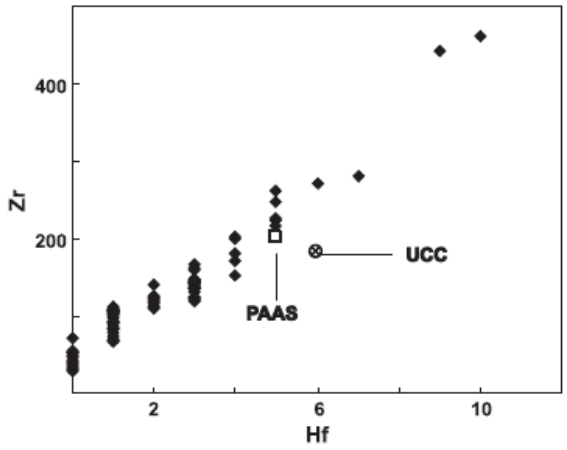

Fig. 9. Binary diagram Zr vs. Hf for the Okavango sediments.

Table 4
The range of elemental ratios in fine sandstones derived from felsic and mafic rocks and comparison with the range for Okavango sediments

Ratio	Fine sandstone		Okavango sediments	CKP11220	CKP10926B	CKP11277	CKP10A299	CKP samples	CKP samples
	Range for sediments from felsic source[a]	Range for sediments from mafic sources[a]	Range	Felsic	Felsic	Mafic	Ultramafic	Felsic n=46	Mafic n=30
Th/Cr	0.13–2.7	0.018–0.046	<0.001–0.75	0.17	0.58	0.01	0.01	0.07–14.50	<0.01–0.50
Th/Sc	0.84–20.5	0.05–0.22	<0.001–2						
Eu/Eu*	0.4–0.94	0.71–0.95	0.3–0.9	0.64	1.23	1.18	0.94	0.28–1.23	0.55–1.22
La/Sc	2.5–16.3	0.43–0.86	0.01–6.7						
La/Co	1.8–13.8	0.14–0.38	0.03–1.39	2.03	1.09	0.21	0.48	0.42–15.18	0.10–1.58

Potential source rocks from NW Botswana also included (CKP suite).
[a] Cullers (2000).

in sample BH8348D (Table 2). The Th concentrations are lower in the Okavango sediments compared to average values in UCC, PAAS and NASC. The range of U and Th/U values in the Okavango sediments encompasses the values obtained from UCC, PAAS and NASC. With the exception of sample BH8159G, which is marked by an extremely low Th/Cr ratio, the Th/Cr ratios for the Okavango sediments overlap values recorded in fine sands/sandstones originating from both felsic and mafic sources (Table 4). Archaean pelites from the Kaapvaal craton in southern Africa are characterised by Th/Cr≤0.02 (e.g., Condie and Wronkiewicz, 1990; Jahn and Condie, 1995), whereas Proterozoic pelites are marked by higher

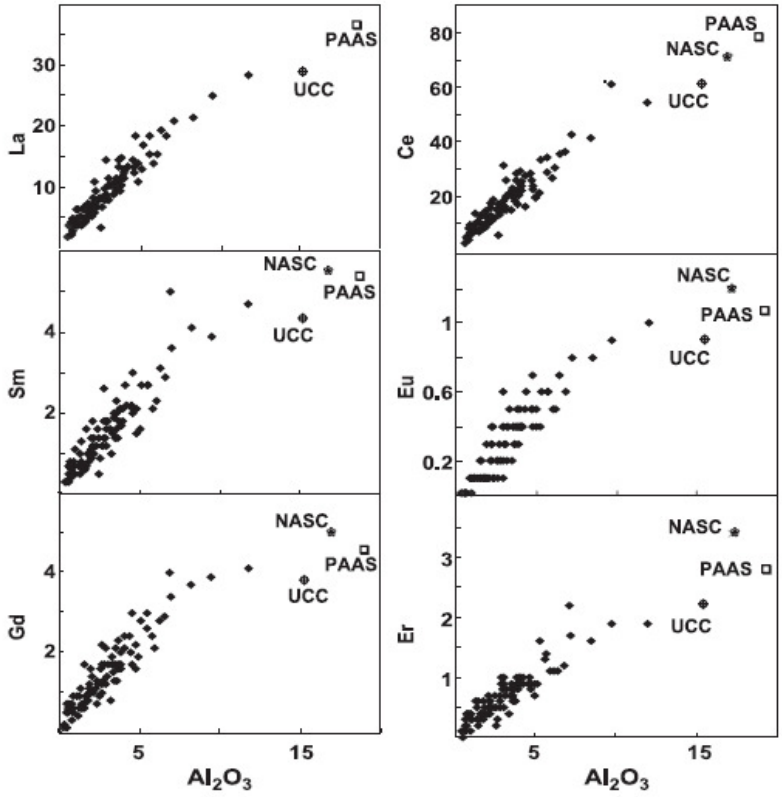

Fig. 10. REE vs. Al_2O_3 diagrams for the Okavango sediments.

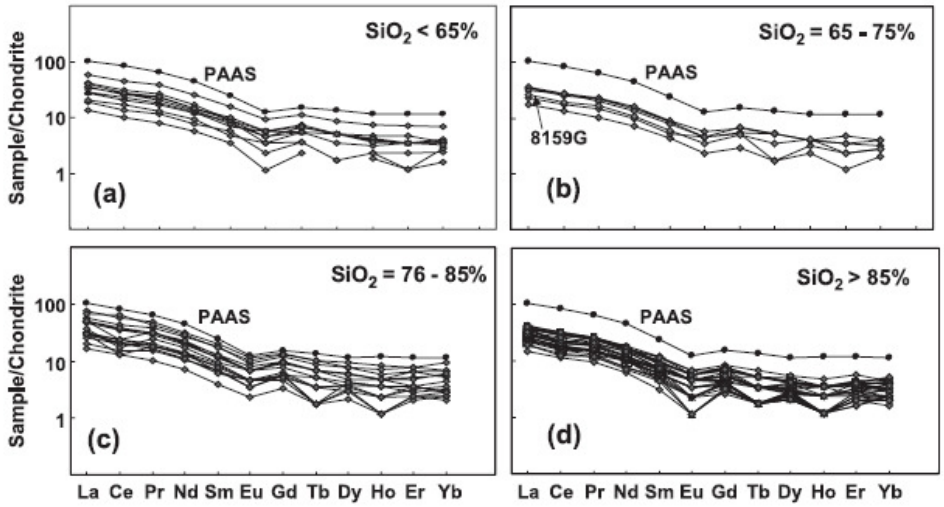

Fig. 11. Chondrite normalized rare earth elements plots of the Okavango sediments. PAAS plotted as a reference.

values, similar to those in the Okavango clastic sediments. With the exception of sample 8159G, the Th/Sc ratios for the Okavango sediments overlap the range of ratios obtained for sediments from felsic and mafic source rocks (Table 4).

7.4. Rare earth elements

The Okavango clastic sediments show a strong positive correlation between individual REE and Al_2O_3 contents (Fig. 10). The rare earth element compositions of these sediments (Table 2) are shown in chondrite-normalized diagrams (Fig. 11). The chondrite-normalized REE pattern of PAAS is also shown in the diagrams for comparison. The REE patterns of the Okavango sediments are characterised by: (1) chondrite-normalized REE values (La_N up to Yb_N) greater than one. The REE patterns show that the Okavango sediments are less enriched in REE than the PAAS; (2) substantial fractionation of light rare earth elements (LREE); (3) flat to slightly fractionated heavy rare earth element (HREE) patterns; (4) a variable Eu-negative anomaly. The sample 8159G displays REE contents similar to values in Okavango sediments with the same SiO2 content (Table 2). The range of Eu/Eu* for the Okavango sediments overlaps the ranges recorded in clastic sediments from felsic and mafic source rocks (Table 4); (5) a weak to strong negative Ce anomaly in some samples with the majority of samples characterised by Ce/Ce* in the range 0.9–1.2.

The La/Sc ratios of the Okavango sediments overlap the ratios recorded in sediments originating

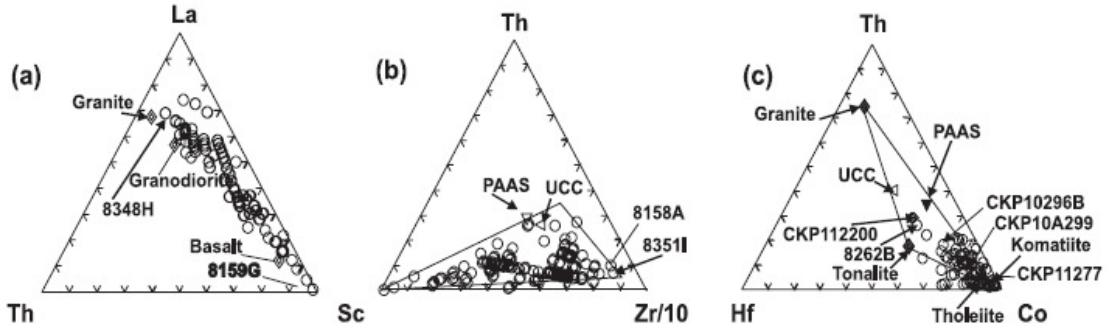

Fig. 12. Geochemical characteristics of the Okavango sediments in the ternary diagrams: (a) La–Th–Sc showing a single evolution trend; (b) Th–Sc–Zr/10 and (c) Th–Hf–Co. Note that the Okavango sediment sample BH8262B overlaps with the composition of the Proterozoic granitoids sample CKP11220 from NW Botswana, suggesting that these granitoids could be the source of this sediment.

from felsic and mafic source rocks (Table 4). La/Co ratios for the Okavango sediments include low values similar to those recorded in sediments from mafic sources and higher values (up to 1.39 in sample 8262B) requiring either an intermediate composition source or a contribution from both mafic and felsic source rocks.

Wronkiewicz and Condie (1987) indicated that the source rock lithology (mafic, intermediate or felsic) strongly influences the concentrations of Th, Sc, La, Zr, Hf and Co in the siliciclastic sedimentary rocks. The relationships between these elements were used to devise ternary diagrams for the identification of the nature of the source rocks of siliciclastic sedimentary rocks. In the diagrams La–Th–Sc (Fig. 12a), Th–Sc–Zr (Fig. 12b) and Th–Hf–Co (Fig. 12c), the Okavango sediments define evolutionary trends or a field extending from mafic to felsic source rock end-members. Since these elements do not enter in the structure of quartz, these trends/fields exclude the aeolian sand component of the sediments. The samples BH8158A and BH8351I plot outside that evolution trend in the Th–Sc–Zr diagram, being displaced towards the Zr apex.

8. Discussion

8.1. Introduction

Several factors control the chemical composition of elements in siliciclastic sedimentary rocks. The most commonly documented are diagenesis, metamorphism, grain-size and density-controlled hydraulic sorting, petrological composition of the source rocks, degree of weathering of the source area and the tectonic setting (e.g., Nesbitt and Young, 1982; McLennan et al., 1983; Wronkiewicz and Condie, 1987; Roser and Korsch, 1988; Camiré et al., 1993; Cullers, 1994a; Fedo et al., 1996; Bock et al., 1998).

Metamorphic remobilisation is excluded for the studied samples because the Okavango sediments are unconsolidated. The first major geochemical complexity of the Okavango sediments is that they show variable content of CO_2, reflecting variable amounts of diagenetic carbonate minerals and organic matter (organic C in the range ~0–1.64 wt.%; authors, unpublished data). Carbonates induce a variable dilution on the clastic component of the studied sediments. However, this study places emphasis on major, trace and ratios of elements hosted in silicate minerals because when processing or plotting the chemical composition of elements involved in the structure of carbonates (e.g., CaO and MgO), emphasis was on carbonate-free samples. The second major geochemical complexity of the Okavango sediments is that they contain a variable but important amount of quartz that induces a drastic variation of SiO_2 contents. This silica dilution effect induces strong variation on all trace element contents (expressed in ppm). To overcome this complexity, this paper places emphasis on interelement ratios and ternary diagrams involving elements that do not enter into the structure of quartz. Most of the discussion below concentrates on unravelling the complex factors controlling the geochemical characteristics of the Okavango sediments in terms of provenance excluding the aeolian sand component.

The Okavango alluvial fan is a nascent (Quaternary) rift, and the half-graben is amagmatic (Modisi et al., 2000). Thus, there is no input of young, weakly weathered volcanoclastic material in the Okavango sediments. Therefore, this paper focuses on the remaining four main factors discussed below.

8.2. Grain-size and density-controlled sorting

The Okavango Delta sediments, including all the samples studied, are well sorted fine to medium-grained sands, with variable amounts of carbonates and minor silt and clay (Table 1 and DWA (Department of Water Affairs), 1997). The Okavango River water constitutes the major source of the fine fraction of the sediments (McCarthy and Ellery, 1995).

A number of studies comparing the chemical composition of fine and coarse clastic sediments from the same source showed that fine sediments are particularly rich in clay minerals and preferentially concentrate elements entering in the structure of mafic minerals in igneous rocks (e.g., Cullers, 1994a,b). Coarser sediments contain a higher proportion of quartz and alkali feldspars. In the Okavango sediments, quartz induces a dilution that is shown by the decrease of all elements with the increase of silica in carbonate-free sediments (e.g., Figs. 5a and 7g,h). As stated above, the quartz

dilution effect explains the large variation of the concentration of the individual trace elements (e.g., 25-fold for Co). Note that the variation of interelement ratios is smaller if samples with abnormal contents for some elements (e.g., 8159G) are excluded. More complex compositional variation occurs in clastic sediments when heavy minerals such as zircon, apatite, monazite and titanite are concentrated in some stratigraphic units due to density-controlled hydraulic sorting. Such units will be enriched in some elements entering in the structure of those heavy minerals. In the Okavango sediments, the two samples showing a relatively high content of Zr (BH8158A and BH8351I) are also marked by high Hf and HREE (e.g., Yb) abundances, indicating a minor hydraulic concentration of zircon. In the ternary diagram Th–Sc–Zr (Fig. 12b), these samples are displaced towards the Zr-apex, indicating a higher amount of zircon compared to other Okavango sediment samples. Monazite is characterised by high abundances of LREE correlated with high contents of P_2O_5. This mineral and related geochemical trend has not been found in the Okavango sediments. Chemical analyses of bulk suspended solids led Sawula et al. (1992) to suggest that TiO_2-rich phases (e.g., titanite) were probably among the solid phases transported by the Okavango floodwater. However, our microscopic and XRD data and a detailed scanning electron microscope (SEM) investigation of Okavango sediments conducted by McCarthy and Ellery (1995) did not record TiO_2-rich phases. The excellent correlation between Al_2O_3 and TiO_2 (Fig. 3b) suggests that both elements are hosted within clay minerals, as previously pointed out by McCarthy and Ellery (1995). Thus, concentration of heavy minerals is not the main factor controlling the chemical variation of the Okavango sediment composition, although zircon concentration does occur in a few samples.

8.3. Source area weathering and diagenetic processes

K-feldspar is the only feldspar detected in five out of 11 samples examined for XRD. The apparent absence of plagioclase may be due to its somewhat lower resistance during transport and weathering. The occurrence of both kaolinite and K-feldspar suggests an advanced weathering source. This is supported by the absence of any mafic minerals, which are generally less resistant to weathering. Calcite and dolomite cements are diagenetic. McCarthy and Metcalfe (1990) estimated that 113,000 $t \cdot a^{-1}$ of $CaCO_3$ and 135,000 $t \cdot a^{-1}$ of SiO_2 are accumulating in the Okavango Delta as a result of subsurface precipitation, as opposed to 40,000 $t \cdot a^{-1}$ of clastic sediment. Thus, chemical precipitation is currently a major depositional process in the Okavango basin.

Investigations of siliciclastic sedimentary rocks in several regions of the world show that their chemical composition is largely inherited from the composition of the weathering profiles at the source of sediments (Nesbitt and Young, 1982, 1984, 1989; Nesbitt et al., 1996). Nesbitt and Young (1982) devised the chemical index of alteration (CIA) which provides a good measure of the degree of alteration of the sediments' source rocks. CIA value in the main rock-forming minerals (quartz, plagioclase, alkali feldspars, pyroxene and olivine) is ≤55. Clay minerals yield higher CIA values (usually ≥75), with the highest value (~100) recorded in kaolinite. Shales are characterised by CIA values ~70–75, which reflect the predominance of clay minerals in their composition. The Okavango sediments are marked by a large range of CIA values (52–81) and a negative correlation of SiO_2–Al_2O_3 (Fig. 5a). These trends reflect a substantial quartz±feldspar dilution-effect.. Petrographic studies (Fig. 3 and Table 1) support this observation since the Okavango sediments are predominantly made of quartz sand. CIA values ≥80 in sedimentary rocks are indication of a source severely affected by chemical weathering. The Okavango sediments contain kaolinite as the dominant clay mineral, and McCarthy and Ellery (1995) suggest that illuviation of fines, including clays, from the floodwater, into preexisiting aeolian sand occurs beneath frequently flooded areas in the lower Delta.

In the A–CN–K diagram (Fig. 6), the Okavango sediments define an evolution trend similar to soils developing above igneous bedrocks. However, in the case of the Okavango sediments, this trend should be interpreted with caution, especially when the origin of sediments is considered. The data in Fig. 6 can be interpreted using a mixing model involving two components: (1) a strongly weathered component plotting close to the A-apex (e.g., sample BH8262C). Kaolinite, which is the most abundant

clay in the Okavango sediments (Table 1), plots at this apex; (2) a relatively immature component which predominates in the sediments plotting closer to the igneous trend line (e.g., sample BH8159A and BH8158A). Important to keep in mind is that none of the studied samples is a pristine end-member since all the Okavango Delta sediments contain a large proportion of sand but both end-members defined above should be located along the mixing line shown in Fig. 6. The component marking a source area severely affected by chemical weathering corresponds to the sedimentary fraction transported by the river from the Angolan hinterlands to the Okavango basin. The component from a weakly weathered source area corresponds to the currently active aeolian component of the Okavango sediments. An important observation from these data is that the geochemical trend in the A–CN–K diagram (Fig. 6) does not, in this case, reflect a progressive unroofing of a weathering profile as is commonly the case in sedimentary rocks (e.g., Nesbitt and Young, 1984, 1989). Therefore, caution should be exercised when interpreting the source area paleo-weathering process, using geochemical data from sedimentary packages containing an aeolian input. In such cases, CIA values, evolution trends in A–CN–K diagrams and various other geochemical indicators could underestimate the importance of chemical weathering at the source for the component of the sediment transported by rivers from wetter regions and entering in a sedimentary basin located in a semiarid region.

The range of negative Ce anomalies reported in the Okavango sediment samples may have been associated with the process of soil formation at the source. Changing pH and oxidation state within the weathering profile allows fractionation of REE, leading to the formation of a range of Ce/Ce* (e.g., Duddy, 1980; Braun et al., 1990).

8.4. Source rock lithology

The combination of aeolian and fluviatile processes in the Okavango sedimentary records implies a diversity of potential source rock components. Several workers showed that a number of chemical elements are not fractionated by exogene processes and therefore could be used for the identification of sediments source rock lithologies (e.g., Taylor and McLennan, 1985; McLennan et al., 1990). The most important among these elements are REE, HFSE and some transition metals (e.g., Cr, Co and Ni). However, Duddy (1980) and Condie et al. (1995) showed that REE are in some cases redistributed in weathering profiles. Redox-dependent Ce-negative anomalies observed in the Okavango sediments are also an indication of fractionation of this element during weathering, fluvial transportation and/or deposition in the basin. Dupré et al. (1996) documented the composition of suspended and dissolved loads and bedloads of the Congo River and showed complex variation trends for REE. For example, there is an inverse correlation between river-dissolved REE with pH (especially at pH>6.5), and a similar correlation has been reported world-wide (e.g., Goldstein and Jacobsen, 1987; Elderfield et al., 1990). However, REE, HFSE and the above transition metals are usually immobile elements concentrated in weathering minerals formed in soils after removal of mobile elements such as the alkali earths. Therefore, these immobile elements are transferred mainly as suspended sediments to the depositional site of sediments. This is supported by the fact that REE, HFSE and transition metal concentrations are up to 10,000 times higher in the suspended load compared to the dissolved load in the major rivers of the world (Goldstein and Jacobsen, 1988; Dupré et al., 1996). Therefore, the concentrations of these elements in sedimentary rocks are mainly controlled by their abundances in the clay fraction of suspended sediments. This is supported by the composition of the Okavango sediments showing excellent correlations between REE and Al_2O_3 (Fig. 10), indicating that the REE is hosted in clay minerals. In this paper, the relationship between immobile elements (REE, HFSE and the transition metals Cr, Co, Ni and V) is used to constrain the source rock lithologies.

V, Cr, Co and Ni are compatible elements during igneous fractionation processes and are generally "depleted" in felsic rocks and "enriched" in mafic–ultramafic rocks. Cr and Ni levels in the Okavango samples are generally lower than in PAAS (cf. silica dilution effect in the Okavango sediments), with the exception of one sample, BH8159G, containing extremely high concentrations of transition metals and MgO (4.5 wt.%), requiring either an ultramafic

source or strong adsorption of transition elements on clays or organic matter during deposition or both. XRD data indicated that this sample contains "V-muscovite". As stressed above, submicroscopic muscovite sensu stricto is rather uncommon in sedimentary rocks, and much of the fine-grained "micaceous" material in sediments is made of muscovite–smectite mixed layers (Deer et al., 1992). Furthermore, it is known that lateritic horizons above ultramafic rocks contain smectites (e.g., Trescases, 1997), and presumably, muscovite–smectite mixed layers as inferred to occur in sample 8159G could accommodate high Cr and Ni contents. The concentration of Al_2O_3 in this sample is relatively low (<2 wt.%), indicating that adsorption on clays is unlikely. The authors' unpublished organic carbon analysis of sample BH8159G (1.02 wt.%) indicates that the high-transition metal content of this sample is not related to an abnormally high abundance of organic carbon. Thus, the most likely interpretation is that the source area lithologies of the Okavango sediments include ultramafic rocks. Cr and Ni show strong positive correlation with MgO and a negative correlation with SiO_2 in the Okavango sediments. These trends support the presence of ultramafic–mafic rocks at the source of the sediments. The contribution of felsic source rocks is required by the presence of quartz and kaolinite (after feldspars) in the sediments and by the high content of silica in several samples (Table 1). The plot of Cr vs. Ni (Fig. 7c) and several other binary plots (e.g., Figs. 5c,e,f, 7g,h and 8a) show two distinct trendlines, indicating three distinct source end-member compositions. One of these three components is the felsic end-member marked by Cr and Ni concentrations clustered close to the origin of the axes in Fig. 7c. The other end-members are two distinct mafic–ultramafic source rocks, one marked by higher Cr content (pyroxene-rich component) and the other marked by higher Ni abundances (olivine-rich component).

The relative contribution of felsic and ultramafic–mafic rock sources should be reflected in the distribution of Zr and Cr–Ni, as these elements monitor zircon from felsic rocks and chromite/pyroxene/olivine from mafic–ultramafic rocks (e.g., Wronkiewicz and Condie, 1987). Co, Ni and Ti abundances are higher in mafic to intermediate rocks, whereas Y and Zr are higher in felsic rocks (e.g., Ishiga and Dozen, 1997). The Cr/Zr ratio is expected to decrease if zircons are concentrated by hydraulic sorting in the sedimentary process. The Cr/Zr ratios in the Okavango sediments (Table 3) show a large range, from low values, 0.04 (e.g., sample BH8158F), identical to values in sediments originating from a felsic source rock, up to high values, ~1.4 (sample BH8162D), reflecting a predominantly mafic source rock. The high Cr/Zr value of ~13 in sample BH8159G indicates ultramafic source rocks. Most Okavango sediments have Cr/Zr between these two end-members, indicating a source made of bimodal felsic/mafic rocks and/or intermediate rocks. A similar conclusion is reached using Y/Ni ratios that are identical to values in sediments from felsic sources for sample BH8348F and from an ultramafic–mafic source for sample BH8159G. The Okavango sediments are commonly marked by values intermediate between these two end-members.

The ternary plots La–Th–Sc, Th–Sc–Zr and Th–Hf–Co (Fig. 12) have been used to deduce the composition of sediments source rocks (Bhatia, 1983; Taylor and McLennan, 1985; Bhatia and Crook, 1986; Camiré et al., 1993; Jahn and Condie, 1995). Th is typically concentrated in felsic rocks, whilst Sc, although a member of the same group (III) of the periodic table, is more concentrated in mafic rocks. This is due to the much smaller size of the Sc ion, allowing it to enter early crystallizing pyroxenes (Taylor and McLennan, 1985). The Okavango sediments define a single evolutionary trend in the La–Th–Sc, supporting a bimodal ultramafic–mafic and felsic source rock association. The nonquartz component of sample BH8159G, marked by extremely high Sc, Cr and Ni, represents a sedimentary material produced almost exclusively from ultramafic–mafic rocks, whereas that in the sample BH8348H corresponds to a sedimentary material originating almost exclusively from felsic rocks. The range of Eu/Eu* values for sands/sandstones derived from felsic and mafic sources partly overlaps, and the Eu/Eu* ratios for samples BH8159G and BH8348H (Table 3) fall in the common field to sediments from mafic and felsic source rocks. In addition, the range of Eu/Eu* in Okavango Delta sediments (Table 3) also requires both felsic and ultramafic–mafic source rocks. Important to note is that, in Fig. 12c, the composition of the sample BH8262B overlaps with that of the sample CKP11220, which represents Proterozoic granitoids

exposed in NW Botswana and in adjacent countries (Angola and Namibia). These granitoids represent a potential felsic end-member source rock lithology for the Okavango sediments.

The distribution of analyses in the diagrams Th–Sc–Zr (Fig. 12b) and Th–Hf–Co (Fig. 12c) supports the involvement of at least three distinct source rocks for the Okavango sediments. Quantitative modelling (Table 5) was performed using analyses of potential source rocks from the catchment area (Kampunzu, unpublished data) represented by CKP11220 and CKP10926B (granite), CKP11277 (gabbro) and CKP10A299 (ultramafic rock). In this quantification, quartz (SiO_2) was used as one additional mixing component to accommodate the aeolian input, and carbonates (CaO–MgO) were used to accommodate diagenetic calcite/dolomite components. In sediments containing substantial diagenetic carbonates where CaO–MgO were added during quantification, higher least square values were obtained probably because the CO_2 content of carbonates was not taken into consideration. Otherwise, the results from the mixing calculations in carbonate-poor samples yield calculated compositions (Table 5) matching the compositions of Okavango Delta sediments, as shown by least square values of <1. This indicates that the CKP samples listed above represent realistic potential source rocks for the Okavango sediments.

Table 5
Results from quantitative modelling using major and REEs

Sample	Composition	Least squares
8157f	15% CKP 11220	0.99
	4% CKP 10296B	
	81% SiO2	
8158f	9% CKP 11220	0.42
	91% SiO2	
8158h	11% CKP 11220	0.83
	1% CKP 10A299	
	3% CKP 10296B	
	85% SiO2	
8159g without Al_2O_3	18% CKP 11277	7.8
	15% CKP 10A299	
	11% CKP 10296B	
	45% SiO2	
	3% MgO	
	8% CaO	
8162k	12% CKP 11220	1.8
	2% CKP 11277	
	7% CKP 10296B	
	78% SiO2	
	1% CaO	
8159t	4% CKP 11220	1.7
	5% CKP 11277	
	4% CKP 10A299	
	1% CKP 10296B	
	82% SiO2	
	1% MgO	
	3% CaO	

9. Conclusions

The Okavango sediments are mainly sands, with variable proportions of silt, clays and carbonates and show a large variation of most elements. The chemical index of alteration displays a continuous trend and a large range from low CIA values (52) marking minimal chemical weathering corresponding to the currently active aeolian component of the Okavango sediments up to high CIA values (81) indicating severe chemical weathering corresponding to a sedimentary fraction transported by the river from the Angolan hinterlands to the Okavango basin.

Elemental compositions, binary diagrams (e.g., Cr–Ni, V–Ni, Ni–SiO_2, Cr–SiO_2, K_2O–Al_2O_3 and Na_2O–Al_2O_3), interelements ratios (e.g., Cr/Zr, Y/Ni, Th/Cr, Th/Sc, Eu/Eu*, La/Sc and La/Co) and source-rock discrimination diagrams (e.g., Th–Sc–Zr and Th–Hf–Co), supported by quantitative modelling, indicate that the Okavango sediments originate from the mixing of aeolian quartz, diagenetic carbonates and a component derived from three distinct source rock groups, including ultramafic–mafic and felsic source rock association, with or without input of intermediate source rocks. Proterozoic granitoids and mafic–ultramafic rocks exposed in NW Botswana and in adjacent countries (Angola and Namibia) represent source rocks for the Okavango sediments.

Acknowledgements

This research project was funded by the University of Botswana Research and Publication Fund (RP 680-

063). The Botswana Geological Survey is acknowledged for allowing us to sample the boreholes used for this study. Water Resources Consultants is acknowledged for assistance with grain size data. A. Jellema is acknowledged for assistance with Fig. 2 and J. J. Tiercelin and D. Kolokose for assistance with the thin sections. This is a contribution to SAFARI 2000 Research Project. The satellite image used in this paper was acquired through that project. This paper benefited significantly from comprehensive reviews by R. Cullers, K. Condie, A. Morton and the Chief-Editor K.A.W. Crook, to whom we extend our thanks.

This paper is dedicated to the memory of Prof. A.B. Kampunzu, a friend, colleague, and mentor, whose profound knowledge, enthusiasm, and desire to help others will continue to be an inspiration to all.

References

Bhatia, M.R., 1983. Plate tectonics and geochemical composition of sandstones. J. Geol. 91, 611–627.

Bhatia, M.R., Crook, K.A.W., 1986. Trace element characteristics of graywackes and tectonic setting discrimination of sedimentary basins. Contrib. Mineral. Petrol. 92, 181–193.

Bock, B., McLennan, S.M., Hanson, G.N., 1998. Geochemistry and provenance of the Middle Ordovician Austin Glen Member (Normanskill Formation) and the Taconian Orogeny in New England. Sedimentology 45, 635–655.

Braun, J.J., Pagel, M., Muller, J.P., Bilong, P., Michard, A., Guillet, B., 1990. Cerium anomalies in laterite profiles. Geochim. Cosmochim. Acta 54, 791–795.

Camiré, G.E., Laflèche, M.R., Ludden, J.N., 1993. Archaean metasedimentary rocks from the northwestern pontiac subprovince of the Canadian shield; chemical characterization, weathering and modelling of the source areas. Precambrian Res. 62, 285–305.

Carney, J.N., Aldiss, D.T., Lock, N.P., 1994. The geology of Botswana. Geol. Surv. Dep., Lobatse, Botswana, p. 113.

Condie, K.C., Wronkiewicz, D.J., 1990. A new look at the Archean–Proterozoic boundary: sediments and the tectonic setting constraint. In: Naqvi, S.M. (Ed.), Precambrian Continental Crust and its Economic Resources. Elsevier, Amsterdam, pp. 61–84.

Condie, K.C., Dengate, J., Cullers, R.L., 1995. Behaviour of rare earth elements in a paleoweathering profile on granodiorite in the Front Range, Colorado, USA. Geochim. Cosmochim. Acta 59, 279–294.

Cullers, R.L., 1994a. The controls on the major and trace element variations of shales, siltstones, and sandstones of Pennsylvanian–Permian age from uplifted continental blocks in Colorado to platform sediment in Kansas, USA. Geochim. Cosmochim. Acta 58, 4955–4972.

Cullers, R.L., 1994b. The chemical signature of source rocks in size fractions of Holocene stream sediment derived from metamorphic rocks in the Wet Mountains region, USA. Chem. Geol. 113, 327–343.

Cullers, R.L., 2000. The geochemistry of shales, siltstones and sandstones of Pennsylvanian–Permian age, Colorado, USA: implications for provenance and metamorphic studies. Lithos 51, 181–203.

David, K., Schiano, P., Allègre, C.J., 2000. Assessment of the Zr/Hf fractionation in oceanic basalts and continental materials during petrogenetic processes. Earth Planet. Sci. Lett. 178, 285–301.

Deer, W.A., Howie, R.A., Zussman, J., 1992. An Introduction to the Rock-Forming Minerals, 2nd ed. Longman Group Limited, Essex, England. 696 pp.

Dickinson, W.R., Suczec, C.A., 1979. Plate tectonics and sandstone compositions. Am. Assoc. Pet. Geol. Bull. 63, 2171.

Duddy, I.R., 1980. Redistribution and fractionation of rare earth and other elements in a weathering profile. Chem. Geol. 30, 363–381.

Dupré, B., Gaillardet, J., Rousseau, D., Allègre, C.J., 1996. Major and trace elements of river-borne material: the Congo Basin. Geochim. Cosmochim. Acta 60, 1301–1321.

DWA (Department of Water Affairs), 1997. Appendix B: geomorphology and sedimentology. Maun Groundwater Development Project Phase 1. Water Affairs Department, Gaborone, Botswana. prepared by Eastend Investments.

Elderfield, H., Upstill-Goddard, R., Sholkovitz, E.R., 1990. The rare earth element in rivers, estuaries, and coastal seas and their significance to the composition of ocean waters. Geochim. Cosmochim. Acta 54, 971–991.

Fedo, C.M., Eriksson, K.A., Krogstad, E.J., 1996. Geochemistry of shales from the Archaean (~3.0 Ga) Buhwa Greenstone Belt, Zimbabwe: implications for provenance and source-area weathering. Geochim. Cosmochim. Acta 60, 1751–1763.

Gao, S., Wedepohl, K.H., 1995. The negative Eu anomaly in Archean sedimentary rocks: implications for decomposition, age and importance of their granitic sources. Earth Planet. Sci. Lett. 133, 81–94.

Garver, J.I., Royce, P.R., Smick, T.A., 1996. Chromium and nickel in shale of the Taconic foreland: a case study for the provenance of fine-grained sediments with an ultramafic source. J. Sediment. Res. 100, 100–106.

Goldstein, S.J., Jacobsen, S.B., 1987. The Nd and Sr isotopic systematics of river-water dissolved material: implications for the sources of Nd and Sr in seawater. Chem. Geol. 66, 245–272.

Goldstein, S.J., Jacobsen, S.B., 1988. Rare earth elements in river waters. Earth Planet. Sci. Lett. 89, 35–47.

Gromet, L.P., Dymek, R.F., Haskin, L.A., Korotev, R.L., 1984. The "North American shale composite": its compilation, major and trace element characteristics. Geochim. Cosmochim. Acta 48, 2469–2482.

Hassan, S., Ishiga, H., Roser, B.P., Dozen, K., Naka, T., 1999. Geochemistry of Permian–Triassic shales in the Salt Range, Pakistan: implications for provenance and tectonism at the Gondwana margin. Chem. Geol. 158, 293–314.

Ishiga, H., Dozen, K., 1997. Geochemical indications of provenance change as recorded in Miocene shales: opening of the Japan Sea, San'in region, southwest Japan. Mar. Geol. 144, 211–228.

Jahn, B.M., Condie, K.C., 1995. Evolution of the Kaapvaal Craton as viewed from geochemical and Sm–Nd isotopic analyses of intracratonic pelites. Geochim. Cosmochim. Acta 59, 2239–2258.

Kampunzu, A.B., Akanyang, P., Mapeo, R.B.M., Modie, B.N., Wendorff, M., 1998a. Geochemistry and tectonic significance of Mesoproterozoic Kgwebe metavolcanic rocks in northwest Botswana: implications for the evolution of the Kibaran Namaqua–Natal Belt. Geol. Mag. 133, 669–683.

Kampunzu, A.B., Bonhomme, M.G., Kanika, M., 1998b. Geochronology of volcanic rocks and evolution of the Cenozoic Western branch of the East African rift system. J. Afr. Earth Sci. 26, 441–461.

Kampunzu, A.B., Armstrong, M.P., Modisi, M.P., Mapeo, R.B., 1999. The Kibaran belt in southwest Africa: ion microprobe U–Pb zircon data and definition of the Kibaran Ngami belt in Botswana, Namibia and Angola. Gondwana Res. 2, 571–572.

Kampunzu, A.B., Armstrong, R.A., Modisi, M.P., Mapeo, R.B.M., 2000. Ion microprobe U–Pb ages on single detrital zircon grains from Ghanzi Group: implications for the identification of a Kibaran-age crust in northwestern Botswana. J. Afr. Earth Sci. 30, 579–587.

Lahtinen, R., 2000. Archaean–proterozoic transition: geochemistry, provenance and tectonic setting of metasedimentary rocks in central Fennoscandian Shield, Finland. Precambrian Res. 104, 147–174.

Le Gall, B., Tshoso, G., Jourdan, F., Féraud, G., Bertrand, H., Tiercelin, J.J., Kampunzu, A.B., Modisi, M., Dyment, J., Maia, M., 2002. Ar–Ar geochronology and structural data from the Okavango giant mafic dike swarm, Karoo large igneous province, N Botswana. Earth Planet. Sci. Lett. 202, 595–606.

Mapeo, R.B.M., Armstrong, R.A., Kampunzu, A.B., 2000. Ages of detrital zircon grains from Neoproterozoic siliciclastic rocks in Shakawe area: implications for the evolution of the Proterozoic crust in northern Botswana. S. Afr. J. Geol. 103, 156–161.

Mapeo, R.B.M., Armstrong, R.A., Kampunzu, A.B., 2001. Ion microprobe U–Pb zircon geochronology of gneisses from the Gweta borehole, NE Botswana: implications for the Paleoproterozoic Magondi belt in southern Africa. Geol. Mag. 138, 299–308.

McCarthy, T.S., Ellery, W.N., 1995. Sedimentation on the distal reaches of the Okavango fan, Botswana, and its bearing on calcrete and silcrete (Ganister) formation. J. Sediment. Res., Sect. A Sediment. Pet. Proc. 65, 77–90.

McCarthy, T.S., Metcalfe, J., 1990. Chemical sedimentation in the semi-arid environment of the Okavango Delta, Botswana. Chem. Geol. 89, 157–178.

McCarthy, T.S., Stanistreet, I.G., Cairncross, B., 1991. The sedimentary dynamics of active fluvial channels on the Okavango fan, Botswana. Sedimentology 38, 471–487.

McCarthy, T.S., Green, R.W., Franey, N.J., 1993. The influence of neo-tectonics on water dispersal in the northeastern regions of the Okavango swamps, Botswana. J. Afr. Earth Sci. 17, 23–32.

McCarthy, T.S., Cooper, G.R.J., Tyson, P.D., Ellery, W.N., 2000. Seasonal flooding in the Okavango Delta, Botswana—recent history and future prospects. S. Afr. J. Sci. 96, 25–33.

McLennan, S.M., Taylor, S.R., Eriksson, K.A., 1983. Geochemistry of Archean shales from the Pilbara Supergroup, Western Australia. Geochim. Cosmochim. Acta 47, 1211–1222.

McLennan, S.M., Taylor, S.R., McCulloch, M.T., Maynard, J.B., 1990. Geochemistry and Nd–Sr isotopic composition of deep sea turbidites: crustal evolution and plate tectonic associations. Geochim. Cosmochim. Acta 54, 2015–2050.

Modisi, M.P., 2000. Fault system of the southeastern boundary of the Okavango Rift, Botswana. J. Afr. Earth Sci. 30, 569–578.

Modisi, M.P., Atekwana, E.A., Kampunzu, A.B., Ngwisanyi, T.H., 2000. Rift kinematics during the incipient stages of continental extension: evidence from nascent Okavango rift basin, northwest Botswana. Geology 28, 939–942.

Nesbitt, H.W., Young, G.M., 1982. Early Proterozoic climates and plate motions inferred from major element chemistry of lutites. Nature 299, 715–717.

Nesbitt, H.W., Young, G.M., 1984. Prediction of some weathering trends of plutonic and volcanic rocks based on thermodynamic and kinetic considerations. Geochim. Cosmochim. Acta 48, 1523–1534.

Nesbitt, H.W., Young, G.M., 1989. Formation and diagenesis of weathering profiles. J. Geol. 97, 129–147.

Nesbitt, H.W., Young, G.M., McLennan, S.M., Keays, R.R., 1996. Effect of chemical weathering and sorting on the petrogenesis of siliciclastic sediments, with implications for provenance studies. J. Geol. 104, 525–542.

Plank, T., Langmuir, C.H., 1998. The chemical composition of subducting sediment and its consequences for the crust and mantle. Chem. Geol. 145, 325–394.

Reeves, C.V., 1978. The gravity survey of Ngamiland: 1970–71. Geol. Surv. Botsw., Bull. 11, 84 pp.

Ringrose, S., Huntsman-Mapila, P., Kampunzu, A.B., Downey, W., Coetzee, S., Vink, B., Matheson, W., Vanderpost, C., 2005. Sedimentological and geochemical evidence for palaeo-environments in Makgadikgadi sub-basin, in relation to the MOZ rift depression, Botswana. Palaeogeogr. Palaeoclimatol. Palaeoecol. (in press).

Roser, B.P., Korsch, R.J., 1988. Provenance signatures of sandstone–mudstone suites determined using discriminant function analysis of major-element data. Chem. Geol. 67, 119–139.

Sawula, G., Martins, E., Nengu, J., Themner, K., 1992. Notes on trace metals in the Boro River, Okavango Delta. Botsw. Notes Rec. 24, 135–149.

Taylor, S.R., McLennan, S.M., 1985. The Continental Crust: Its Composition and Evolution. Blackwell Scientific, Oxford. 312 pp.

Taylor, S.R., McLennan, S.M., 1995. The geochemical evolution of the continental crust. Rev. Geophys. 33, 241–265.

Thomas, D.S.G., Shaw, P.A., 1991. The Kalahari Environment. Cambridge University Press, Cambridge. 284 pp.

Toulkeridis, T., Clauer, N., Kröner, A., Reimer, T., Todt, W., 1999. Characterization, provenance, and tectonic setting of Fig Tree

greywackes from the Archaean Barberton Greenstone Belt, South Africa. Sediment. Geol. 124, 113–129.

Trescases, J.-J., 1997. The lateritic nickel–ore deposits. In: Paquet, H., Clauer, N. (Eds.), Soils and Sediments. Mineralogy and Geochemistry. Springer Verlag, Berlin, pp. 125–138.

Wronkiewicz, D.J., Condie, K.C., 1987. Geochemistry of Archean shales from the Witwatersrand Supergroup, South Africa: source-area weathering and provenance. Geochim. Cosmochim. Acta 51, 2401–2416.